AD-A114 902 ROCKWELL INTERNATIONAL THOUSAND OAKS CA SCIENCE CENTER F/G 1/3
VISCOUS-INVISCID INTERACTIONS OVER TRANSONIC TANGENTIALLY BLOWN--ETC(U)
APR 82 N D MALMUTH, W D MURPHY, J D COLE N00014-81-C-0104
UNCLASSIFIED SC5296.1FR NL

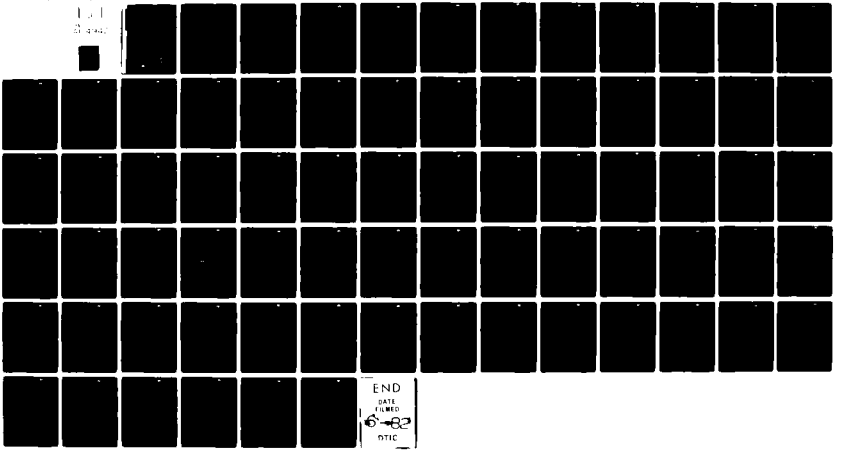

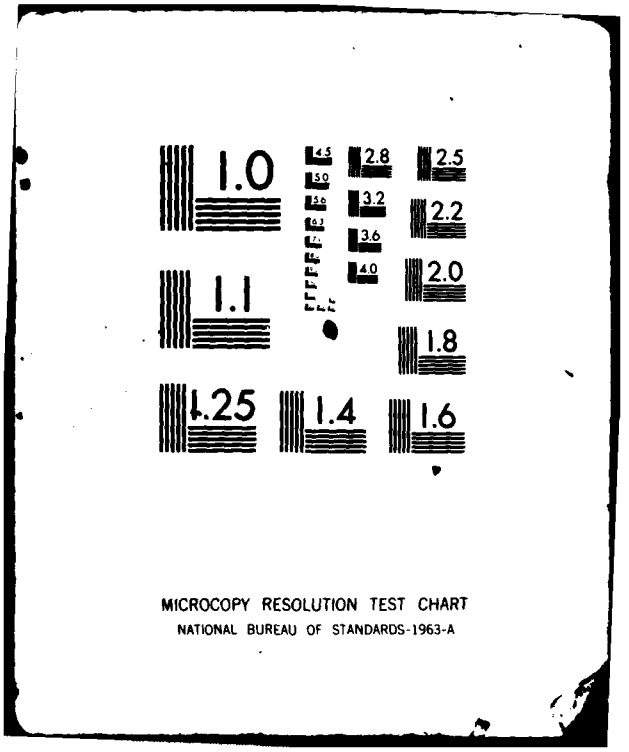
1.0
1.1
1.25
1.4
1.6
1.8
2.0
2.2
2.5
2.8
3.2
3.6
4.0
4.5
5.0
5.6
MICROCOPY RESOLUTION TEST CHART
NATIONAL BUREAU OF STANDARDS-1963-A

Report No. SC5296.1FR

VISCOUS-INVISCID INTERACTIONS OVER TRANSONIC TANGENTIALLY BLOWN AIRFOILS

N.D. Malmuth, W.D. Murphy
Rockwell International Science Center
Thousand Oaks, California 91360

and

J.D. Cole
University of California at Los Angeles
Los Angeles, California 90024

April, 1982

Final Report for Period February 16, 1981 through February 15, 1982

Prepared for

Office of Naval Research
800 N. Quincy Street
Arlington, VA 22217

This research was sponsored by the office of Naval Research under Contract No. N00014-81-C-0104

UNCLASSIFIED

SECURITY CLASSIFICATION OF THIS PAGE (When Data Entered)

REPORT DOCUMENTATION PAGE		READ INSTRUCTIONS BEFORE COMPLETING FORM
1. REPORT NUMBER	2. GOVT ACCESSION NO. AD-A124 942	3. RECIPIENT'S CATALOG NUMBER
4. TITLE (and Subtitle) VISCOUS-INVISCID INTERACTIONS OVER TRANSONIC TANGENTIALLY BLOWN AIRFOILS		5. TYPE OF REPORT & PERIOD COVERED Final report for period 02/16/81 thru 02/15/82
		6. PERFORMING ORG. REPORT NUMBER SC5296.1FR
7. AUTHOR(s) N.D. Malmuth, W.D. Murphy and J.D. Cole		8. CONTRACT OR GRANT NUMBER(s) N00014-81-C-0104
9. PERFORMING ORGANIZATION NAME AND ADDRESS Rockwell International Science Center P.O. Box 1085 Thousand Oaks, California 91360		10. PROGRAM ELEMENT, PROJECT, TASK AREA & WORK UNIT NUMBERS
11. CONTROLLING OFFICE NAME AND ADDRESS Office of Naval Research 800 N. Quincy Street Arlington, VA 22217		12. REPORT DATE April, 1982
		13. NUMBER OF PAGES 63
14. MONITORING AGENCY NAME & ADDRESS(if different from Controlling Office) Office of Naval Research 800 N. Quincy Street Arlington, CA 22217		15. SECURITY CLASS. (of this report) Unclassified
		15a. DECLASSIFICATION DOWNGRADING SCHEDULE

16. DISTRIBUTION STATEMENT (of this Report)

Approved for public release; distribution unlimited.

17. DISTRIBUTION STATEMENT (of the abstract entered in Block 20, if different from Report)

18. SUPPLEMENTARY NOTES

None

19. KEY WORDS (Continue on reverse side if necessary and identify by block number)

Transonic flow, jets, lift, propulsion systems, augmenter wings, viscid-inviscid interactions, wall jets, partial differential equations, numerical analysis, computational fluid dynamics, asymptotic analysis.

20. ABSTRACT (Continue on reverse side if necessary and identify by block number)

A viscous interaction model has been developed for the treatment of tangentially blown transonic airfoils. The coupling procedure employs a small disturbance approximation for the nearly inviscid outer flow and interacts this region with the boundary layer, wall jets, and propulsive wake. Keller's box scheme is utilized to treat these viscous zones. On the basis of parametric studies for laminar flow, the skin friction drag appears to increase nearly linearly with the blowing coefficient C_J for a fixed Mach number-incidence

DD FORM 1 JAN 73 1473

UNCLASSIFIED

SECURITY CLASSIFICATION OF THIS PAGE (When Data Entered)

combination, giving a substantial scrubbing drag penalty for "overblowing" beyond the C_J necessary to achieve attached flow. Increases in wave drag over the same range of C_J are much smaller. Associated supercirculation gains with overblowing are inefficient from the standpoint of L/D due to the large values of scrubbing drag. The role of surface skin friction in modifying the viscous cambering of the airfoil in the laminar case is compared to a turbulent modification of the coupling model. Whereas the laminar results show a lift increase associated with the cambering action of the wall jets, the turbulent solutions indicate a decambering effect resulting in decreased lift. Also evident with the turbulent results are increased skin friction and wave drag. A explanation of these trends in terms of the Karman momentum equation is given.

TABLE OF CONTENTS

		Page
	FOREWORD	iv
	SUMMARY	v
	NOMENCLATURE	vi
1.0	INTRODUCTION	1
2.0	MODEL FORMULATION	4
	2.1 Interacted Inviscid Problem	6
	2.2 Interacted Viscous Problem	12
3.0	NUMERICAL PROCEDURES	19
4.0	RESULTS	27
5.0	CONCLUSIONS	56
6.0	RECOMMENDATIONS	59
7.0	REFERENCES	61

LIST OF TABLES

Table		Page
1.	Comparison of overall forces on blown NACA 0012 airfoil, $M_\infty = 0.7$, $\alpha = 1°$, $C_J = 0.047$, $Re = 10^6$, $x_{SL} = 0.19$	38
2.	Effect of blowing on separation point, $M_\infty = 0.8$, $\alpha = 1°$	43
3.	Effect of Reynolds number Re and slot location on aerodynamic characteristics, $M_\infty = 0.75$, $\alpha = 1°$, $C_J = 0.0371$	47

LIST OF ILLUSTRATIONS

Figure		Page
1a.	Regions of considerations for tangentially blown airfoil	5
1b.	Regions for interacted inviscid boundary value problem	5
2.	Flow diagram of algorithm	26
3.	Convergence of coupling procedure, NACA 0012 airfoil, $M_\infty = 0.75$, $\alpha = 2°$, $C_J = 0.04$	29
4.	Variation of integral thicknesses, peak velocity (f'_{max}) and skin friction coefficient C_f for $M_\infty = 0.75$, $\alpha = 1°$, $C_J = 0.055$ on upper surface of blown NACA 0012 airfoil	31
5.	Streamwise development of boundary layer and wall jet velocity profiles over airfoil. Profiles for upper surface shown in upper part of figure; lower surface values in lower part of figure	33
6.	Streamwise development of velocity profiles in wake for $M_\infty = 0.75$, $\alpha = 1°$, $C_J = 0.055$	34
7.	Effect of blowing coefficient C_J on chordwise pressure distributions, $M_\infty = 0.75$, $\alpha = 1°$	35
8.	Comparison of laminar and turbulence blown chordwise pressures with inviscid theory $M_\infty = 0.7$, $\alpha = 1°$, $C_J = 0.047$, $Re = 10^6$, $x_{SL} = 0.19$, (NACA 0012 airfoil)	37
9.	Comparison of $\delta^*(x)$'s for turbulent and laminar flows, $M_\infty = 0.7$, $\alpha = 1°$, $C_J = 0.047$, $Re = 10^6$, $x_{SL} = 0.19$, (NACA 0012 airfoil)	39
10.	Effect of blowing on drag coefficients	41
11.	Skin friction drag versus wave drag for varying blowing (arrows hereinafter denote blowing increasing)	42
12.	Fraction of total drag associated with various blowing rates and flight conditions	45

LIST OF ILLUSTRATIONS

Figure		Page
13.	Effect of blowing on lift	46
14.	Effect of blowing on L/D = $C_L/\left(C_{D_{wave}} + C_{D_f}\right)$	48
15.	Modifications of lift and drag with blowing	49
16.	Variation of aerodynamic efficiency with lift coefficient at various flight conditions	50
17.	Curvature of velocity profile at wall for varying blowing, $M_\infty = 0.75$, $\alpha = 1°$, (upper surface)	53
18.	Variation of shape factor, H downstream of slot (0.19ℓ) for NACA 0012 airfoil, $M_\infty = 0.75$, $\alpha = 1°$, (upper surface)	54

FOREWORD

This report summarizes research conducted under the contract N00014-81-C-0104, "Viscous Interactions over Transonic Tangentially Blown Wings," during the period 16 February 1981 through 15 February 1982. The effort was sponsored by the Office of Naval Research.

SUMMARY

A viscous interaction model has been developed for the treatment of tangentially blown transonic airfoils. The coupling procedure employs a small disturbance approximation for the nearly inviscid outer flow and interacts this region with the boundary layer, wall jets, and propulsive wake. Keller's box scheme is utilized to treat these viscous zones. On the basis of parametric studies for laminar flow, the skin friction drag appears to increase nearly linearly with the blowing coefficient C_J for a fixed Mach number-incidence combination, giving a substantial scrubbing drag penalty for "overblowing" beyond the C_J necessary to achieve attached flow. Increases in wave drag over the same range of C_J are much smaller. Associated supercirculation gains with overblowing are inefficient from the standpoint of L/D due to the large values of scrubbing drag. The role of surface skin friction in modifying the viscous cambering of the airfoil in the laminar case is compared to a turbulent modification of the coupling model. Whereas the laminar results show a lift increase associated with the cambering action of the wall jets, the turbulent solutions indicate a decambering effect resulting in decreased lift. Also evident with the turbulent results are increased skin friction and wave drag. An explanation of these trends in terms of the Karman momentum equation is given.

NOMENCLATURE

$A_{\substack{u \\ \ell}}$	Slot blowing parameters
C	Chapman constant
C_o	Constant for pressure representation near nose
C_j	Blowing coefficient
C_μ	Scaled blowing coefficient
C_L	Lift coefficient
$C_{D_{WAVE}}$	Wave drag
C_{D_f}	Friction drag
C_f	Skin friction coefficient
d	Slot height
$F_{\substack{u \\ \ell}}$	Boundary of airfoil surface
$f_{\substack{u \\ \ell}}$	Boundary of airfoil surface, reduced stream function
g	Quantity appearing in definitions of integral thicknesses
h	Quantity appearing in definitions of integral thicknesses, mesh spacing
I	Integral appearing in turbulence model
I_1	Integral appearing in turbulence model
J	Momentum flux
K	Transonic similarity parameter
k	Mesh spacing
L	Lift
ℓ	Airfoil chord
M_∞	Freestream Mach number
m	Factor appearing in definition of c

m_1	Coefficient appearing in viscous momentum equation
m_2	Coefficient appearing in viscous momentum equation
n	Coordinate in direction of outward surface normal
Q	Quantity appearing in definition of integral thicknesses
Re	Freestream Reynolds number
s	Coordinate in direction of parallel to surface
u	Velocity component along parallels to wall, also $f'(\eta)$
v	$f''(\eta)$
$x,\tilde{y}$	Cartesian coordinates
α	Angle of attack
δ	Thickness ratio
δ^*	Displacement thickness
ϵ	Wake displacement
ϵ^+	Eddy viscosity
Γ	Circulation
η	Transformed vertical coordinate
η_d	Scaled slot height
θ	Momentum thickness
λ	Algebraic turbulence model parameter
κ	Algebraic turbulence model parameter
μ	Viscosity
ρ	Density
ϕ	Perturbation potential
ψ	Stream function
Ω	Vorticity
Ω_T	Total vorticity
τ	Jet deflection angle

Subscripts

A	Airfoil
e	Edge of viscous layer
u	Upper
ℓ	Lower
FF	Far field
max	Maximum value
SL	Slot
te	Trailing edge
W	Wake
∞	Freestream quantity

Superscripts

U	Upper
ℓ	Lower
n	Iteration counter

Special Symbols

$\langle\ \rangle$	Average
[ ]	Jump

1.0 INTRODUCTION

Achievement of separation-free flow has been an intrinsic pacing item in obtaining high lift characteristics for airfoils and wings. At low speeds, this capability is extremely important to the Navy from the viewpoint of carrier take-off and landing performance, operation from bombed-out runways as well as fleet dispersal requirements. From a tactical viewpoint, it is also significant in high-speed maneuver scenarios. Associated with existing threats, combat in the transonic Mach number regime will continue to be important for the indefinite future. In typical dogfights, a substantial advantage is obtained with turn-radius reduction while maintaining high speed and excess thrust. Accordingly, aerodynamic efficiency can play an important role in mission survivability.

The attainment of high lift at transonic speeds is impacted by shock-induced separation. Tangential blowing using engine air, ducted through a chamber, exhausting gas along the wing surface has been suggested as a means of coping with this problem, by accelerating the flow to overcome the shock induced adverse pressure gradients. In quantifying the blowing requirements to obtain separation-free flow as well as giving information relevant to optimized aerodynamic design of blown wings, computational models can play an important role. Although the low speed problem has received considerable attention since the early work of Spence in Ref. 1, the viscous-interaction problem has not been intensively analyzed. However, recently, there have been studies amalgamating panel methods with parabolized Navier stokes solvers to treat viscid-inviscid interactions over jet-flapped airfoils for the incompressible case as exemplified by Ref. 2. To treat shock waves and other nonlinear effects arising in the transonic regime, other procedures are required. In this connection, Refs. 3-5 give inviscid solutions for jet-flapped airfoils and wings as well as upper surface blown airfoils. These solutions can be utilized as the initial iterate for the nearly inviscid portion of the flow in a Prandtl weak interaction procedure to handle

attached cases appropriate to moderate amounts of blowing. In Refs. 6 and 7 the initial iterate of the blown boundary layer or wall jet portion of these flows is described. Therein, other theoretical developments - associated with treatment of wave interactions in wall jet flows are also provided. This work was performed under the auspices of an ONR Contract N00014-76-C-0350 during the period January 1976 through March 1981 with the objective of modeling flows in transonic wall jets and blown airfoils.

This report will describe the generalization of the models given in Refs. 3-7 to handle viscous interactions over blown transonic airfoils. As such, it is a summary of work performed under ONR Contract N00014-81-C-0104 during the period 16 February 1981 through 15 February 1982. Contained in this document is a description of the theoretical formulations employed and a discussion of results arising from the computational flow solutions. The thrust will be to treat the impact of the coupling process on the external nearly inviscid flow field. Effects on the airfoil characteristics will also be treated, including the influence on the circulation of jumps in pressure and normal velocity in the wake as well as blown portions of the airfoil. Also included in this analysis is the attendant alteration of the far field due to the modified vorticity in the wake. With this methodology, the connection between blowing and maintenance of separation-free flow will be discussed in the light of parametric examples. Questions involving the impact of blowing on achieving laminar flow, minimum friction drag, shock-free flow and optimum force characterisitics will also be addressed.

Because of the multiple extrema inherent in the wall jet velocity profiles, difference rather than integral methods have been utilized herein to compute the viscous regions of the flow. Although integral methods can represent substantial time savings in the computation, and have therefore proven of great value, their empiricism, intrinsic arbitrariness, and indifference to the actual details of the wall jet velocity

profile development can represent distinct disadvantages in understanding blown flows with emphasis on tradeoffs between separation control, the different forms of drag, and the development of high lift. In regard to the coupling procedure, the method employed in this analysis is an extension of those described in Refs. 8-12 to blowing. For solution of the wall jet and wake, the box scheme as described in Refs. 13-15 has been adapted to solve the relevant initial boundary value problem for the boundary layer as it is modified with tangential injection. The adaptation to wall jets employs concepts that we have developed in earlier three-dimensional incompressible studies. An account of these is given in Ref. 16. In what follows, both laminar and turbulent* boundary layers are discussed, with emphasis on the former.

To treat the inviscid part of the flow, the SLOR procedures of Ref. 17 which is an improvement over that contained in Ref. 18 have been employed in this analysis. The viscous interaction problem is solved also by the SLOR procedure with modifications for the jump conditions in the wake region. Details of these are to be found in what follows.

*The turbulent results were obtained under a Rockwell complementary IR&D program and are included for completeness of the discussion.

2.0 MODEL FORMULATION

A schematic of the tangentially blown transonic airfoil to be considered is shown in Figure 1a. An airfoil is shown with slots S_+ and S_- on its upper and lower surfaces respectively, which introduce air or another gas tangential to the airfoil surface at these locations. Regions (1±) - (4) have special significance that will be discussed presently. This blowing is utilized to overcome the adverse pressure gradient along the surface introduced by shocks or the pressure recovery process as the flow approaches the trailing edge. For laminar flows, and certain airfoils, the lower surface slot is usually required because of the enhanced possibility of separation in these cases.

To obtain the flow over this arrangement, a "zonal" method is utilized as contrasted to a full elliptic Navier stokes procedure. This option has been selected to avoid difficult grid generation issues and lengthy as well as costly computational procedures to provide information useful to design and relevant to the flow structure.

For the zonal approach, a Prandtl viscous-inviscid iteractive scheme is utilized to solve the viscous interaction singular perturbation problem for large Reynolds numbers Re appropriate to practical applications. In this limit, the viscous terms in the gasdynamic equations of motion are negligible except in the boundary layer. For thin airfoils at small incidence, the Karman-Guderley (KG) small disturbance equation can be utilized to describe the flow field in this nearly inviscid "outer" flow region. Referring to Figure 1b, the small disturbance assumptions can be utilized in the usual way also to transfer the flow tangency boundary conditions from the actual airfoil and wake surface to a slit representing an approximate location of the airfoil's upper and lower surfaces and its downstream projection.

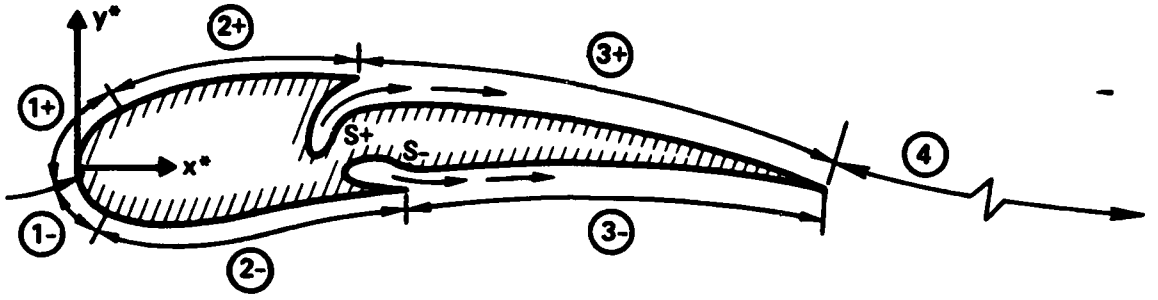

Fig. 1a Regions of consideration for tangentially blown airfoil.

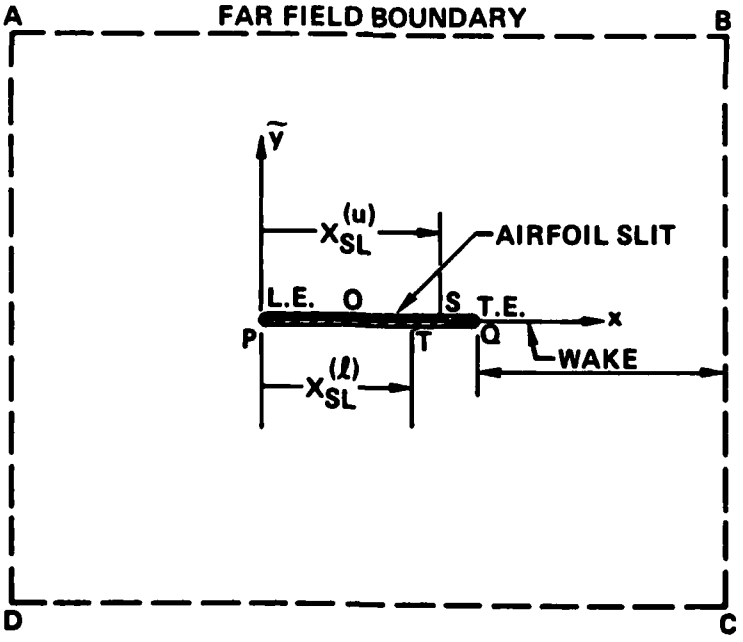

Fig. 1b Regions for interacted inviscid boundary value problem.

2.1 Interacted Inviscid Problem

In the viscous-interaction procedure, the inviscid problem is modified strictly through its boundary conditions. For the small disturbance framework, described here, the KG equation of motion for the perturbation potential ϕ given by

$$[K-(\gamma+1)\phi_x]\phi_{xx} + \phi_{\tilde{y}\tilde{y}} = 0 \quad , \tag{1}$$

valid inside the region bounded externally by the contour ABCD and internally by the slit POQP in Figure 1b is solved subject to these conditions. In (1),

$K = (1-M_\infty^2)/M_\infty\delta^{2/3}$ = small disturbance parameter

δ = airfoil thickness ratio

M_∞ = freestream Mach number

$\tilde{y} = (M_\infty^2\delta)^{1/3}y$,

and x and $\tilde{y}$ are Cartesian coordinates expressed in units of the airfoil chord*, and subscripts denote partial differentiation.

With viscous interactions, on the basis of the generalization of the asymptotic results in Ref. 6 to compressible flow or those described in Ref. 11, the modified boundary conditions can be shown to be

*Slight corrective scalings involving monomials in M_∞ have been introduced in accord with empirical procedures.

$$\left.\begin{aligned} \phi_{\tilde{y}}(x,0+) &= F_u'(x) + \delta^{-1}\frac{d\delta_A^{*(u)}}{dx} \\ \phi_{\tilde{y}}(x,0-) &= F_u'(x) - \delta^{-1}\frac{d\delta_A^{*(\ell)}}{dx} \end{aligned}\right\} \quad 0<x<1 \qquad (2a),\ (2b)$$

$$\left.\begin{aligned} [\phi_x] &\equiv \phi_x(x,0+) - \phi_x(x,0-) = -\delta^{1/3} M_\infty^{3/4}\{\theta_W + \delta_W^*)\epsilon''(x) \qquad (2c) \\ [\phi_{\tilde{y}}] &= \delta^{-1}\frac{d\delta_W^*}{dx} \qquad (2d) \\ \epsilon'(x) &= \langle\phi_{\tilde{y}}\rangle \equiv \tfrac{1}{2}(\phi_{\tilde{y}}(x,0+) + \phi_{\tilde{y}}(x,0-)) \qquad (2e) \end{aligned}\right\} \quad 1<x<x_{FF}$$

primes denoting differentiation with respect to x and where the equations of the airfoil upper and lower surfaces respectively are

$$y = \delta f_u(x) - \alpha x \equiv \delta F_u(x) \qquad (2f)$$

$$= \delta f_\ell(x) - \alpha x \equiv \delta F_\ell(x) \qquad (2g)$$

Here, α denotes the angle of attack and the wake deflection is given by

$$y = \delta\epsilon(x) \quad . \qquad (2h)$$

Also in (2), the quantities $\delta_A^{*(u)}$, $\delta_A^{(\ell)}$, and δ_W^* denote the displacement thickness on the upper, lower surfaces and wake respectively, and θ_W represents the corresponding momentum thickness. These integral thicknesses are defined in Eqs. (12) in what follows.

Additional boundary conditions for the problem (2) are required in the far field $x^2 + \tilde{y}^2 \to \infty$. These are applied on the finite boundary ABCD and are obtained under the assumption that the viscous

far field is explicitly of the same form as the inviscid one, i.e.,

$$\phi \simeq \frac{1}{\pi\sqrt{K}}\left\{\int_0^1 t'(\xi)\ell n|z-\xi|d\xi + \int_0^1 R(z,\xi)[c'(\xi)-A]d\xi - \right.$$

$$\left. + \int_1^\infty R(z,\xi)\,\epsilon'(\xi)d\xi\right\} \tag{3a}$$

where

$$R(z,\xi) = \ell n\left|\frac{(\xi+1)^{\frac{1}{2}} - (z+1)^{\frac{1}{2}}}{(\xi+1)^{\frac{1}{2}} + (z+1)^{\frac{1}{2}}}\right| \tag{3b}$$

$$A \equiv \alpha/\delta$$

and $z = x+i\sqrt{K}\,\tilde{y}$. The quantities c and t denote the camber and thickness functions of the airfoil, i.e., $f_u(x) = c(x) + t(x)$ and and $f_\ell(x) = c(x) - t(x)$. In addition, it is shown that

$$\epsilon'(x) \simeq \sqrt{K}\left\{C_\mu \epsilon'(1) - \Gamma_{te}\right\}/2\pi x \text{ as } x \to \infty \tag{4a}$$

where Γ_{te} the circulation at the trailing edge is determined numerically from

$$\Gamma_{te} = [\phi]_{x=1} \tag{4b}$$

and C_μ is a scaled blowing coefficient such that if C_J is the blowing coefficient defined as

$$C_J = J/q\ell$$

where J is the total momentum flux from the slots, q is the dynamic pressure, ℓ is the chord then,

$$C_\mu = M_\infty^{3/4} \delta^{1/3} C_J \quad .$$

The expansion (4a) is used to evaluate the infinite integral in (3a) outside the computational domain.

The representation (3a) is used as a Dirichlet condition $\phi = \phi_{FF}$ on ABCD. Actually, it includes viscous interactions through the wake vorticity $[\phi_x]$ which for inviscid flow according to Refs. 1, and 5 is related to the wake curvature $\approx \epsilon''(x)$ by the formula

$$[\phi_x] = \frac{C_\mu}{2} \epsilon''(x) \quad . \tag{5}$$

From integration by parts, the last integral on the right hand side of (3a) can be related to the wake vorticity through (5). Actually, (3a) neglects the contribution to the vorticity on the airfoil. This has been assumed to be a small effect in our viscous interaction calculations. For this reason and computational expediency, (3a) was utilized with the viscous effect occurring through updates of $\epsilon'(x)$ from (2e) in the Prandtl iteration process involving Eqs. (2).

A formula which includes vorticity on the wing as well as in the wake is motivated by the picture that in outer inviscid coordinates, the wake is line rather than a layer, and that from Green's theorem as applied in Ref. 3, the blown airfoil-wake combination can still be replaced by a concentrated potential vortex at the origin $x = \tilde{y} = 0$. Accordingly, ϕ_{FF} would be given by

$$\phi_{FF} = \frac{-\Gamma_\infty \theta}{2\pi} \quad \text{as} \quad x^2 + K\tilde{y}^2 \to \infty$$

$$\theta = \tan^{-1} \frac{K^{\frac{1}{2}}\tilde{y}}{x}$$

where

$$-\Gamma_\infty = -[\phi]_{x=\infty} = \Omega_T = \iint_{-\infty}^{\infty} \Omega dx dy \quad ,$$

by Stokes' theorem, in which Γ is the circulation on a circuit at infinity, Ω is the vorticity, Ω_T is the total vorticity, and $[\phi]_{x=\infty}$ is the jump in potential across the wake line. These ideas are consistent with the result (for incompressible flow) in Ref. 20 in which the lift L is given, even for viscous flow by the Kutta-Joukowski law in which if ρ_∞ and U are respectively the free stream density and velocity, then

$$L = \rho_\infty U \Gamma_\infty \quad ,$$

providing that Γ_∞ is the circulation on a circuit at infinity intersecting the wake perpendicularly. Note that in a viscous flow, Γ is circuit dependent, because of the variable vorticity along the wake. In Ref. 21, for a compressible flow, it is shown that

$$L = -\rho_\infty U \Omega_T \quad .$$

In the iterative cycle to be discussed, the first phase of the calculation is to solve the inviscid boundary value problem. At this stage, $\delta_A^{*(u)}$, $\delta_A^{*(\ell)}$ and δ_W^* in Eqs. (2a,b,d) are set to zero and the coefficient of $\epsilon''(x)$ in (2c) is replaced by $C_\mu/2$. For this and subsequent interacted inviscid fields, an additional condition required to make the problem well-posed is the value of $\epsilon'(1)$. Also, (2e) is used as indicated in Section 3.0 since the jet is a free boundary. If τ is the angle that the wake centerline or jet leaves the trailing edge, then

$$\epsilon'(1) = -(\alpha+\tau)/\delta \quad . \tag{6}$$

For a jet flap, i.e., the jet is at the trailing edge, and τ is specified. For tangential blowing, the inviscid condition is applied that the wake centerline for a wedge shaped trailing edge leaves tangent to the higher stagnation pressure surface, which for the cases considered, is on the upper side. Accordingly,

$$\tau = -180\delta\, f_u'(1)/\pi \tag{7}$$

is assumed. In actuality, the lift and some flow details could be affected by this choice and more accurate "multi-deck" viscous local solutions generalizing those of Stewartson and other workers (see Ref. 22) would appear warranted to refine (7).

The foregoing describes essential features of the calculation of the viscous corrections to the primarily inviscid portion of the blown flow. To complete this part of the formulation, viscous corrections to the surface pressures are indicated. These are implemented at the conclusion of the viscid-inviscid iteration sequence and have the forms

$$[\phi_x(x,0+)] = \phi_x(x,0++) - \phi_x(x,0+) = -\delta^{1/3} F_u''(x)\left(\theta_A^{(u)} + \delta_A^{*(u)}\right) \tag{8a}$$

$$[\phi_x(x,0-)] = \phi_x(x,0-) - \phi_x(x,0--) = \delta^{1/3} F_\ell''(x)\left(\theta_A^{(\ell)} + \delta_A^{*(\ell)}\right) \tag{8b}$$

$$\text{for} \quad 0 \leq x < 1$$

where ++ and -- denote the edges of the boundary layer or wall jet over the upper and lower surfaces respectively, and + and - indicate the upper and lower surfaces respectively. At $x = 0$ in the computations, the quantities $\theta_A^{(u)}$, $\theta_A^{(\ell)}$, $\delta_A^{*(u)}$, $\delta_A^{*(\ell)}$ are set to zero.

2.2 Interacted Viscous Problem

To solve the inviscid problem, the integral thicknesses, i.e., δ^*'s and θ's appearing in Eqs. (2) must be determined from the viscous region of the flow. For this purpose, the adaptation of the box scheme to tangential blowing as described in Ref. 6 has been used. To achieve the necessary clustering, a stretched vertical coordinate η is introduced. If (s,n) represents a coordinate system erected respectively along parallels and normals to the airfoil, then,

$$\eta = \rho(u_e/\rho_e\mu_e s_1)^{\frac{1}{2}} n \tag{9}$$

(n is the direction of the outward normal) where ρ is the density, u is the velocity component parallel to the surface, subscript e denotes the edge of the boundary layer, wall jet or wake, μ is the viscosity, and s_1 refers to the distance along the surface from the stagnation point. For thin airfoils, $n \approx |y|$, and $s_1 \approx x$ away from the nose region of a blunt nosed airfoil. These approximations will also be assumed valid on the wake. If the stream function ψ is represented as

$$\psi = (\rho_e\mu_e u_e x)^{\frac{1}{2}} f(\eta,x) \tag{10}$$

then the velocity ratio $u/u_e = \frac{\partial f}{\partial \eta} \equiv f'(\eta,x)$. This leads to the transformed momentum equation

$$(bf'')' + m_1 ff'' - m_2(f'^2) + m_2 c = x\left(f'\frac{\partial f'}{\partial x} - f''\frac{\partial f}{\partial x}\right) \tag{11a}$$

where

$$c \equiv \rho_e/\rho = \frac{1-mf'^2}{1-m} \quad , \quad m \equiv \left(\frac{u_e}{U}\right)^2 /[i+2/(\gamma-1)M_\infty^2] \tag{11b}$$

$$m_2 = \frac{x}{u_e}\frac{\partial u_e}{\partial x} \tag{11c}$$

$$m_1 = (1/2)(1+m_2) \tag{11d}$$

$$b \equiv C(1+\epsilon_m^+) \tag{11e}$$

$$C \equiv (\rho\mu)/\rho_e\mu_e \quad . \tag{11f}$$

Here, ϵ_m^+ is an eddy viscosity which will be discussed later. For laminar flow, $b = 1$. In the solution procedure and in (11b), an adiabatic wall and constant stagnation enthalpy in the blown boundary layer and wake has been assumed. Furthermore, a Chapman gas approximation in which $C = 1$ has also been made.

From this formulation, the integral thickness appearing in Eqs. (2) are given by

$$\delta_A^{*(u)} = Q\int_0^\infty g\,d\eta \tag{12a}$$

$$\delta_A^{*(\ell)} = Q\int_{-\infty}^0 g\,d\eta \tag{12b}$$

$$\delta_W^{*} = Q\int_{-\infty}^\infty g\,d\eta \tag{12c}$$

$$\theta_A^{(u)} = Q\int_0^\infty h\,d\eta \tag{12d}$$

$$\theta_A^{(\ell)} = Q\int_{-\infty}^0 h\,d\eta \tag{12e}$$

$$\theta_W = Q\int_{-\infty}^\infty h\,d\eta \tag{12f}$$

where

$$Q \equiv \left(\frac{x\rho_e}{u_e\rho_\infty Re}\right)^{\frac{1}{2}} \qquad (12g)$$

$$g \equiv c - f' \qquad (12h)$$

$$h \equiv f'(1-f') \qquad (12i)$$

Re = freestream Reynolds number

For numerical purposes, the infinite upper limts $\pm\infty$ appearing in Eqs. (11) and what follows are replaced by $\pm\eta_\infty$, where $\eta_\infty >> 1$ represents edge of the boundary layer, wall jet, or wake.

In accord with the discussion in Ref. 6, the parabolic initial boundary value problem for Eq. (11a) involves the following conditions:

$$f(0,x) = 0 \qquad (13a)$$

$$f'(0,x) = 0 \qquad (13b)$$

$$f'(\infty,0) = 1 \qquad (13c)$$

$$f'(-\infty,0) = 1 \qquad (13d)$$

Over the upper surface and lower surface of the airfoil, the boundary layers in regions ① + ② in Figure 1a are solved subject to (13a,b) as well as (13c) and (13d) respectively. Initial conditions for regions ① + ② are obtained by specializing Eqs. (11) to x = 0 and solving the resulting two point boundary value problem. In this process, the asymptotic solutions in the neighborhood of a finite curvature airfoil nose in the K-G small disturbance theory as well as those for viscous stagnation flow are used to obtain the various coefficients appearing

in (11a) given by Eqs. (11b) - (11d). Further details of this procedure are given in Section 3.0.

The box scheme integration as described in Section 3.0 is continued until the slot locations $x = x_{SL}^{(u)} = x_{SL}^{(\ell)}$ are reached. Thereupon, new initial conditions are applied. For the NACA 0012 laminar cases considered, a slot and tangential injection was required on the lower surface to avoid separation there and thereby permit a fully converged Prandtl iteration sequence. As outlined in Ref. 6, the initial condition of the slots for which $x_{SL}^{(u)} = x_{SL}^{(\ell)} = x_{SL}$ was assumed for the parametric studies employed the marched boundary layer from upstream ($x < x_{SL}$) for $\eta > \eta_d$, and an injection profile which was assumed parabolic*, i.e.

$$f' = A_{u,\ell}(\eta_d - \eta)\eta \quad , \quad 0 \leq |\eta| < |\eta_d| \quad , \tag{14a}$$

where a translation of axes is made such that $\eta = 0$ is the position of the airfoil surface downstream of the slot, u and ℓ refer to upper and lower surfaces respectively, and the slot location is given by $n = d$. In (14), the constants $A_{u,\ell}$ and η_d are related to the blowing coefficient as follows:

$$C_J = (\eta_d^5)(A_\ell^2 + A_u^2)\left(x_{SL}/Re\right)^{\frac{1}{2}}/15 \tag{14b}$$

$$= (16/15)(d/\ell)(\bar{\rho}/\rho_e)\left(f'^{(u)}_{max}{}^2 + f'^{(\ell)}_{max}{}^2\right)$$

where

$$\rho_d = \frac{d}{c}\,(\bar{\rho}/\rho_e)(Re/x_{SL})^{\frac{1}{2}} = \text{transformed slot height} \tag{14c}$$

$$\bar{\rho} = d^{-1}\int_0^d \rho dy = \text{mean density across slot} \tag{14d}$$

*More general distributions could be investigated with our computational model.

and the subscript max refers to the maximum value. The quantity $\bar{\rho}/\rho_e$ above can be used to obtain a temperature effect in modifying C_J. In the calculations reported in Section 4.0, the blowing parameters of the upper and lower slots were made to be the same. Furthermore, A_u, A_ℓ values were sought giving attached flow over the entire airfoil surface. However, when separation did occur for an assumed value of the A_{u_ℓ}, they were increased until fully attached flow conditions were achieved. Results for blowing inadequate to maintain completely attached flow have been used to correlate the separation point x_{sep} against C_J in Refs. 6 and 7 as well as in Section 4.0.

To treat the flow between the slot locations $x = x_{SL}$ and the trailing edge, i.e., Regions ③ in Figure 1a, the initial distributions f" and f in our scheme are obtained by analytic differentiation and integration to supply the portion of the initial data on the line $x = x_{SL}$ lying in the range $0 \leq |n| < |n_d|$. As indicated previously, the part of the initial data on $x = x_{SL}$ lying in the range $|n_d| < |n| \leq |n_\infty|$ is obtained from box scheme values at $x = x_{SL}$ associated with the integration of (11a) from $x = 0$ to x_{SL}. For, Regions ③, the integration process continues until the trailing edge $x = 1$ is reached. There, the integrated solution of the upper surface is combined with that coming from the lower side to provide initial data on the interval $-n_\infty \leq n \leq n_\infty$ for downstream integration of the wake-jet (Region ④ in Figure 1a). The integration continues until the far field boundary BC in Figure 1b is reached, i.e., $x = x_{FF}$. The boundary conditions used in Region ④ are (13a,c,d). Our numerical approach to satisfy them is described in Section 3.0.

Algebraic Eddy Viscosity Model

For the turbulent results described in Section 4.0, the following two layer eddy viscosity model of Patankar and Spalding[23] as well as Ramaprian[24] was used.

First Layer

$$\epsilon_m^+ = (\kappa^2\sqrt{xRe}|f''(\eta)|)I/c^2 \qquad 0\leqslant y\leqslant y^* \qquad (15a)$$

Second Layer

$$\epsilon_m^+ = (\lambda^2\sqrt{xRe}|f''(\eta)|)I_1^2/c^2 \qquad y\geqslant y^* \qquad (15b)$$

where

$$I \equiv \int_0^\eta c\,d\eta$$

$$I_1 \equiv I(\eta_1)$$

$$y^* \equiv (\lambda y_1)/\kappa$$

and η_1 is the first η (beginning at $\eta = \pm\infty$ and proceeding to $\eta = 0$) where

$$|1-f'(\eta_1)| \leqslant 0.01 \quad .$$

The quantities κ and λ in (15) are empirical constants.

In Regions ③, we used typical wall jet values of $\lambda = 0.125$ and $\kappa = 0.435$. For $0\leqslant x \leqslant 0.005$, a laminar model was used. For other regions, we used $\lambda = 0.1$ and $\kappa = 0.4$. More sophisticated models have been proposed involving intermittency and damping corrections as well as a special procedure for wakes. The results in Section 4.0 do not contain these refinements. Instead, Eqs. (15) are used to address some of the more global trends and issues that arise in comparing the turbulent case against the laminar one, particularly, regarding the effect of blowing on aerodynamic characteristics such as lift and drag.

Our computational model however is general enough to assimilate other turbulence simulations.

We note that in the implementation of (15) in the wake region, two intervals of validity of Eq. (15b) are used, i.e., $y_u^* \leq y < \infty$ and $-\infty \leq y \leq y_\ell^*$. In a central region, (15a) is used for which $y_\ell^* \leq y < y_u^*$. Other aspects of the application of (15) involve assuming that $c'(\eta) = 0$ for x stations close to $x = x_{SL}$ and $x = 1$. This measure appears necessary to stabilize the box scheme. Additionally, η_∞ must be made larger in the turbulent case to handle the more rapid growth of the turbulent layer than the laminar one.

3.0 NUMERICAL PROCEDURES

Inviscid (0^{th} Iterate)

The numerical method for solving the interacted inviscid problem comprised by Eqs. (1) - (3) is the standard SLOR of Jameson[17] which includes Murman's[18] fully conservative relaxation (FCR) technique. In the subsonic region, centered differences are employed, while in the supersonic zone, upwind differencing is necessary for stability. The boundary conditions on the airfoil and the far field are incorporated in the usual way. For the wake region, Eq. (5) is integrated to yield

$$[\phi] = \Gamma_{te} + C_\mu \left\{ \epsilon'(x) + (\alpha+\tau)/\delta \right\} /2 \qquad (5')$$

where (4b) and (6) were used.

In our procedure, Eq. (5') is inserted into the discretization of $\phi_{\tilde{y}\tilde{y}}$ at the line above $\tilde{y} = 0$ by replacing $\phi_{i,j-1}$ with

$$\phi_{i,j-1} + \Gamma_{te} + C_\mu \left\{ \epsilon'(x_i) + (\alpha+\tau)/\delta \right\} /2 \quad , \qquad (16a)$$

and at the line below $y = 0$ by replacing $\phi_{i,j+1}$ with

$$\phi_{i,j+1} - \Gamma_{te} - C_\mu \left\{ \epsilon'(x_i) + (\alpha+\tau)/\delta \right\} /2 \quad . \qquad (16b)$$

for $1 < x_i \leq x_{FF}$.

Further details are given in Ref. 4. After each sweep of the grid network, ϵ' is updated using Equation (2e), i.e.,

$$\epsilon'^{(n)}(x_i) = \left(\phi_{i,j}^{(n-1)} - \phi_{i,j-1}^{(n-1)} \right) /(y_j - y_{j-1}) \quad , \qquad (17)$$

where y_j is the first mesh point below the line $\tilde{y} = 0$ and the superscript

n denotes the relaxation sweep counter. Unfortunately, because of the singularity at the trailing edge, Eq. (17) cannot be applied for the first two mesh points to the right of x = 1. Here, $\epsilon'(x_1)$ and $\epsilon'(x_2)$ are determined using an interpolation procedure and Eq. (6), i.e., in which ϵ'_1, and ϵ'_2 are interpolated using $\epsilon'_0 = \epsilon'(1) = -(\alpha+\tau)/\delta$ as well as ϵ'_3, ϵ'_4, ϵ'_5, and ϵ'_6, which are determined from (17). Convergence occurs when the maximum residuals for ϕ, ϵ' and Γ_{te} are all less than 10^{-5}.

Viscous Zones

The boundary layer equations and boundary conditions, (11) and (13) are discretized using Keller's box scheme (13, 14). First, these equations are re-written as a first order system by introducing the new independent variables $u(\eta,x)$ and $v(\eta,x)$, giving

$$f' = u \tag{18a}$$

$$u' = v \tag{18b}$$

$$(bv)' + m_1 fv + m_2(c-u^2) = x\left(u\frac{\partial u}{\partial x} - v\frac{\partial f}{\partial x}\right) \tag{18c}$$

Using Keller's box scheme on a nonuniform grid, (18a, 18b) are discretized as

$$\frac{f_j^n - f_{j-1}^n}{h_j} = u_{j-\frac{1}{2}}^n \tag{19a}$$

$$\frac{u_j^n - u_{j-1}^n}{h_j} = v_{j-\frac{1}{2}}^n \tag{19b}$$

where we have averaged about the point $(x_n, \eta_{j-\frac{1}{2}})$. Using the box centered at $(x_{n-\frac{1}{2}}, \eta_{j-\frac{1}{2}})$, (18c) is discretized as:

$$\frac{(bv)^n_j - (bv)^n_{j-1}}{h_j} + (m_1)_{n-\frac{1}{2}} f^n_{j-\frac{1}{2}} v^n_{j-\frac{1}{2}} + (m_2)_{n-\frac{1}{2}} (c-u^2)^n_{j-\frac{1}{2}}$$

$$+ (x_{n-\frac{1}{2}}) \left[v^n_{j-\frac{1}{2}} \frac{\left(f^n_{j-\frac{1}{2}} - f^{n-1}_{j-\frac{1}{2}}\right)}{k_n} + \frac{v^{n-1}_{j-\frac{1}{2}} f^n_{j-\frac{1}{2}}}{k_n} - \frac{\left(u^n_{j-\frac{1}{2}}\right)^2}{k_n} \right] = s_{n-1} \qquad (19c)$$

where

$$s_{n-1} = \frac{(bv)^{n-1}_{j-1} - (bv)^{n-1}_j}{h_j} - (m_1)_{n-\frac{1}{2}} (fv)^{n-1}_{j-\frac{1}{2}} - (m_2)_{n-\frac{1}{2}} (c-u^2)^{n-1}_{j-\frac{1}{2}}$$

$$- x_{n-\frac{1}{2}} \left(u^{n-1}_{j-\frac{1}{2}} u^{n-1}_{j-\frac{1}{2}} + v^{n-1}_{j-\frac{1}{2}} f^{n-1}_{j-\frac{1}{2}} \right) \Big/ k_n \quad . \qquad (19d)$$

where $h_j = \eta_j - \eta_{j-1}$, and

$k_n = x_n - x_{n-1}$, and $f^n_{j-\frac{1}{2}} = \frac{1}{2}(f^n_j + f^n_{j-1})$, etc.

The boundary conditions become

$$f^n_o = u^n_o = 0 \qquad (19e)$$

$$u^n_j = 1 \qquad (19f)$$

Since the parameters m_1 and m_2 are difficult to compute in the vicinity of the singularity at the nose of the airfoil ($x = 0$), it is

necessary to develop the following local solution* applicable to finite leading edge curvature noses,

$$u_e \approx 1 - \delta^{2/3} C_0/(\sqrt{x^*} + \delta C_0^{2/3})^{2/3}, \quad 0 \leq x^* < x_{C_{p1}} \tag{20a}$$

assuming $U = 1$, $A = O(1)$, and where

$$x^* = (x/1.4845\delta)^2 \tag{20b}$$

for the NACA 00XX series airfoils. The quantity C_0 is obtained by fitting with the numerical solution, i.e.,

$$C_0 = \frac{M_\infty^{2/3} C_p(x_{C_{p1}})\, X_{C_{p1}}^{1/3}}{2\,\delta^{2/3}} \tag{20c}$$

where $x_{C_{p1}}$ is the first mesh point to the right of $x = 0$ and $C_p(x_{p1})$ is the corresponding pressure coefficient (computed numerically) at this mesh point. For $x > x_{C_{p1}}$ a cubic spline fit is sufficient for interpolation of C_p data where

$$u_e = 1 - M_\infty^{3/4} C_p(x^*)/2 \tag{21}$$

for $x^* > x_{C_{p1}}$. Using (20) or (21), m_1 and m_2 may be easily computed from (11c) and (11d).

---

*Note that for $A^{-1} = o(1)$, according to Ref. 25, $\phi_x \sim (\text{sgn } y)x^{*-1/3}$ and C_0 must change sign accordingly.

The discretized system of equations (19) may be solved very efficiently using Newton's method because the Jacobian matrix has a block tri-diagonal structure. Furtermore, the box scheme is second order in a variable grid and can handle discontinuities in the coefficients m_1 and m_2, which are very important at x_{SL}, the shock location, and the trailing edge. See Refs. 13 and 14 for the details.

As indicated in Ref. 26, if the initial condition is not the natural one, then physical disturbances and/or spatial oscillations may occur in the computed solution. At the slot location, it is necessary to damp out these oscillations by using a fine grid ($\Delta x = 0.001$) and averaging over the previous solution (x_{n-1}) for the first five mesh points to the right of x_{SL}. This procedure works well, but has the effect of decreasing the order of the local truncation error in the discretized system from second to first order. Since, however, the mesh has, also been substantially refined no loss of accuracy should result.

In the wake, a three point boundary value problem can be solved at each x station to satisfy (13a,c,d). However, for coding expediency, as outlined in Ref. 6, we used an iterative method related to a suggestion of Cebeci[27] and other iterative schemes we considered in which $f(-\eta_\infty, x) = \gamma(x)$ is iterated on γ until (13a) is satisfied. Here, $\gamma(x)$ is determined by Newton's method to satisfy (13a). The process usually converges in one to three iterations.

More sophisticated treatments are possible in which Goldstein-like layers are interposed near the wake centerline to handle the discontinuity in boundary conditions at $y = 0$ in proceeding from the left to right across $x = 1$, and the associated secondary layer near the wake centerline. An account of one of them for symmetric wakes is given in Ref. 28.

Interacted Inviscid Region

The technique for solving the interacted inviscid region is similar to the SLOR method previously described. The airfoil conditions

(2) are handled similarly. However, on the wake, the jump conditions (2c,d) are incorporated and require special attention. No mesh points appear on the line $\tilde{y} = 0$. The first points above, and below the axis are at $\pm h/2$ and the second points are at $\pm 3h/2$. By Taylor's series and (2c) and (2d)

$$\phi(x,\frac{h}{2}) - \phi(x,\frac{-h}{2}) = [\phi(x,0)] + \frac{h}{2}[\phi_{\tilde{y}}(x,0)] + \Gamma_{te}$$

$$= \Gamma_{te} - \delta^{1/3} M_\infty^{3/4} \int_1^X (\theta_w + \delta_w^*)\epsilon'' dx \qquad (22)$$

$$+ \frac{h}{2\delta} \frac{d\delta_w^*}{dx}$$

where the integral may be evaluated numerically. Equation (22) may now be inserted into the discretized form of $\phi_{\tilde{y}\tilde{y}}$ using the same "trick" given by (16a) and (16b).

Equation (2e) is discretized above and below the $\tilde{y}$-axis, and the resulting expression replaces Eq. (6) for $x \geq x_3$. For x_1 and x_2, the previous interpolation technique must be used because of instabilities created by the singularity at the trailing edge.

The algorithm described above works quite well for laminar problems and no underrelaxation is ever necessary, in contrast to the integral methods described by Lock in Ref. 11. As would be expected, the integral methods for solving the boundary layer problem are faster; however, the boundary layer profiles are much more complicated (multiple extrema) when blowing is introduced, and, consequently, we believe that integrating Eq. (14) using the box scheme is a more accurate approach. The only difficulties in our method sometimes occur at the slot location, trailing edge or at the shock locations at high Mach numbers. The remedy is to use a finer grid in these areas and to smooth the cusped velocity profiles (f') at the slots and trailing edge.

Convergence of the overall problem is defined to occur when the C_L's from two complete viscous-inviscid cycles converge to 0.001. A flow diagram of our algorithm appears in Figure 2.

SC82-17524

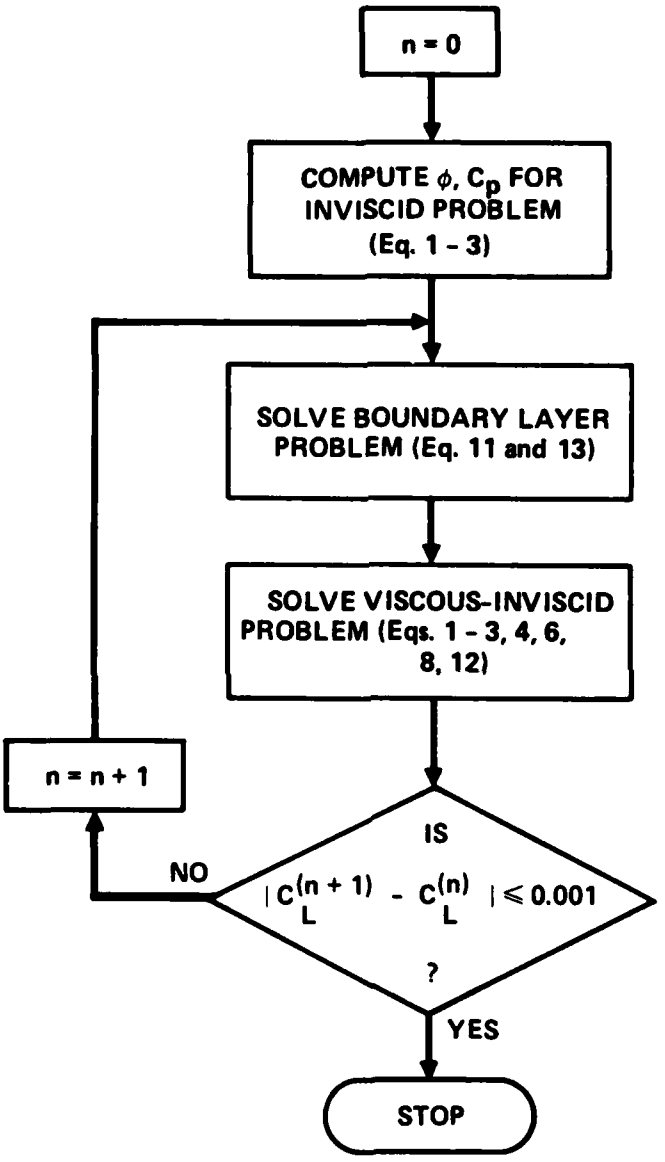

Fig. 2 Flow diagram of algorithm.

4.0 RESULTS

To illustrate the effect of viscous interactions on the performance of tangentially blown airfoils, the coupling procedure described in previous sections was applied to a NACA 0012 airfoil primarily within laminar flow environments. In this study, the influence of such parameters as Mach number, incidence, blowing coefficient, Reynolds number and slot position on the aerodynamic characteristics was investigated.

A solution library including approximately 25 cases has been developed which has rather extensive information regarding the flow fields for these varying conditons. From it, typical results have been selected and discussed herein to highlight trends and issues of engineering significance. It will be clear that they are also relevant to more fundamental concerns regarding flows over blown wings. Some of these are:

- The structure of jet-wakes, particularly their effective velocity and impact on the global supercirculation and lift
- The genesis and control of wave and friction drag in blown transonic flows
- Growth properties and momentum budgets of wakes from propulsive wings, invariances associated with these budgets and deviations from self similitude for coflowing, jets as compared to free and self-propelled jets
- Blown Kutta condition
- Stability and transition of wall jets and tangentially blown flows over airfoils and wings

- The structure of the nearly inviscid far field and its asymptotic matching to the near field

- Multiple decks near the jet exit and trailing edge, breakdown of boundary layer approximations and wave interactions inside wall jets and mixing layers.

Because separation phenomena were not considered in the analysis, the results for the unblown case will not be included in this discussion. For this reason, and as suggested previously, it was also necessary to introduce blowing on the lower surface to overcome the adverse pressure gradients typically present for this particular airfoil, even at zero incidence. Configurations with blowing on the lower surface as well as the upper one relate to transonic applications of augmenter wings and other schemes for high lift development at these Mach numbers.

A question of some importance in the utilization of the coupling scheme indicated in Figure 2 is the number of viscous-inviscid interations required for convergence of the coupling. In Figure 3, chordwise pressure distributions for a typical laminar case are shown for the NACA 0012 airfoil at $M_\infty = 0.75$, $\alpha = 2°$, and a blowing coefficient $C_j = 0.04$ with the upper and lower slots at 19% chord. As indicated in Figure 2, the initial iterate is the inviscid blown solution. This gives rise to the pressures shown in Figure 3. Subsequent couplings move the terminating shock for the supersonic region rearward. The results show that the convergence of the viscous-inviscid cycle is extremely rapid, requiring only two iterations in this case. Two to three iterations was typical for all of the approximately 25 cases studied. In this connection, it is interesting and important to note that the introduction of blowing provides a new opportunity to study weak interactions not generally accessible to difference methods for the transonic unblown case, unless inverse procedures are used and other special measures such as backward marching and degenerate forms of the boundary layer equations are employed to treat the

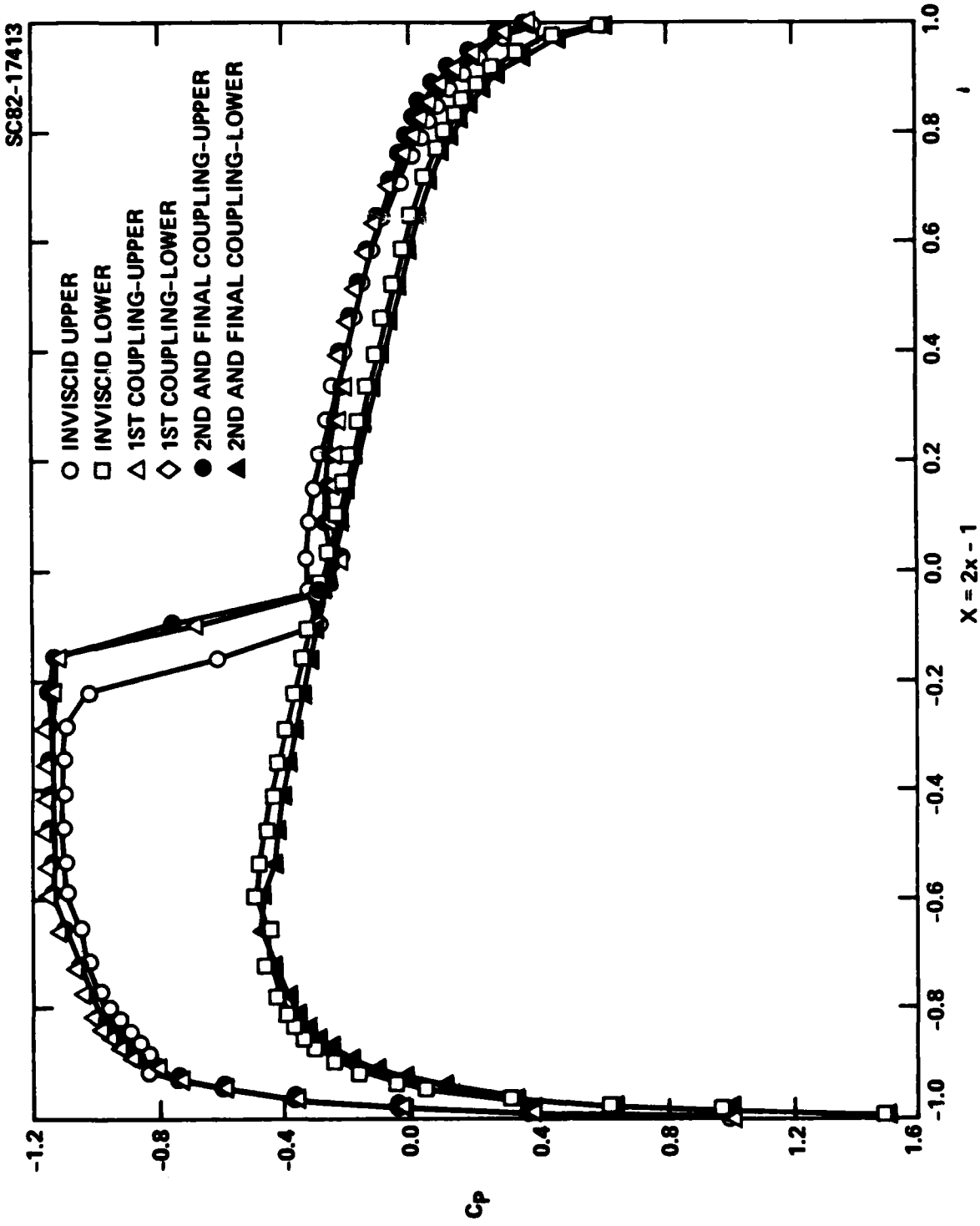

Fig. 3 Convergence of coupling procedure, NACA 0012 airfoil, $M_\infty = 0.75$, $\alpha = 2^0$, $C_J = 0.04$.

attendant separated regions. The significance of this aspect is that it may allow investigation of the treatment of the trailing edge-near wake region in an unseparated context and therefore enable us to understand its matching to the external flow more easily.

Another feature of the laminar distributions shown in Figure 3 is the fact that they exemplify a case in which the viscous lifting pressures are actually higher than the "inviscid" values. This somewhat surprising result which differs as will be seen from the corresponding turbulent flow contrasts with the unblown case in which viscosity reduces the lift. Interpretation of this finding relates partially to the viscous character of the inviscid blowing model. This can be appreciated from the asymptotic thin jet analysis given in Ref. 5 which is a generalization and asymptotic formalization of that given by Spence in Ref. 1. In this connection, it appears questionable whether the latter is the infinite Reynolds number limit of the weak interaction theory formulated in this report. Another more important factor relates to the change in sign of the wall jet displacement and momentum thicknesses and their streamwise slopes associated with blowing as compared to a conventional boundary layer. According to the transpiration boundary conditions (2a,b), this can result in an effective cambering and incidence change induced by the wall jets and jet wakes as contrasted to the decambering action of conventional boundary layers for the unblown case. A qualitative discussion of this mechanism is given in Ref. 20. Along with the cambering tendency, the negative displacement thicknesses result in thinning of the profile as contrasted to thickening occurring with ordinary boundary layers. The former is illustrated in Figure 4, where displacement and momentum thicknesses δ_A^* and θ_A over the upper surface of the NACA 0012 airfoil are shown along with the local skin friction coefficient and peak velocity variations for the $M_\infty = 0.75$, $\alpha = 1°$, $C_j = 0.055$ case. At the slot location, $x = 0.19$, the quantities jump, related to the mass flow from the slot. Downstream of this location, the displacement thickness δ_A^*

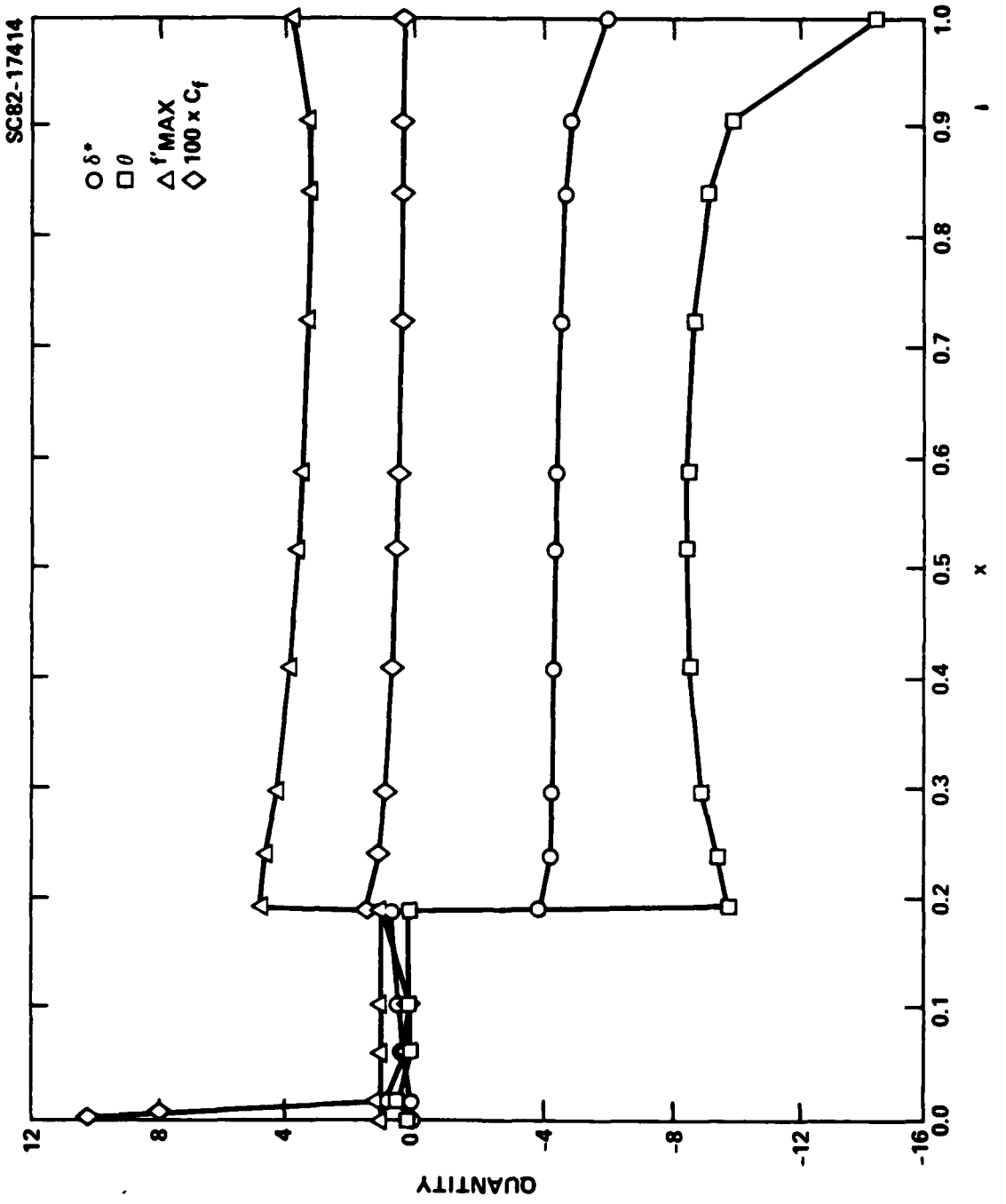

Fig. 4 Variation of integral thicknesses, peak velocity (f'_{max}) and skin friction coefficient C_f for $M_\infty = 0.75$, $\alpha = 1^0$, $C_J = 0.055$ on upper surface of blown NACA 0012 airfoil.

obtained from Eqs. (12) is negative, related to the excess velocity wall jet which contrasts to the defect boundary layer encountered in the unblown case. In addition, negative $\delta_A^{*\prime}(x)$ variations are apparent between the slot and trailing edge relevant to the aforementioned sink-like action. Associated with this behavior of the integral thicknesses is the streamwise evolution of the velocity profiles $f'(\eta)$ depicted in Figure 5. Here, the plus and minus signs refer to conditions immediately downstream and upstream of the slot, respectively. Analogous development is shown in Figure 6 for the trailing edge and wake ($x > 1$) profiles. Although not attempted in this investigation, this information can be used to perform a study of the effect of the viscous interaction on transonic thrust recovery, and has a bearing also on the development of the wake vorticity, curvature, and circulation as they affect lift. In Ref. 6, the asymptotic development of the wake profile to a nearly universal bell shape profile is discussed. Similarities and differences of the present application to flat plate wakes as well as free and self-propelled jets are described therein.

In Figure 7, the effect of blowing coefficient on the surface pressures is shown. It is evident that there is a pronounced rearward motion of the terminating shock on the upper surface associated with increased blowing. This is consistent with the idea that the latter cambers the upper surface. The associated increase in lift, wave drag, and skin friction drag will be discussed shortly.

In connection with the integral thicknesses, an evaluation of the correctness of the parabolic solver was made by checking their compatibility with the integral form of the momentum equation, i.e.,

$$\frac{d\theta}{dx} = \overbrace{\frac{\tau}{\rho_e u_e^2}}^{C_f} - \overbrace{\frac{\theta}{u_e}\frac{du_e}{dx}(2+H-M_e^2)}^{P} \qquad (23a)$$

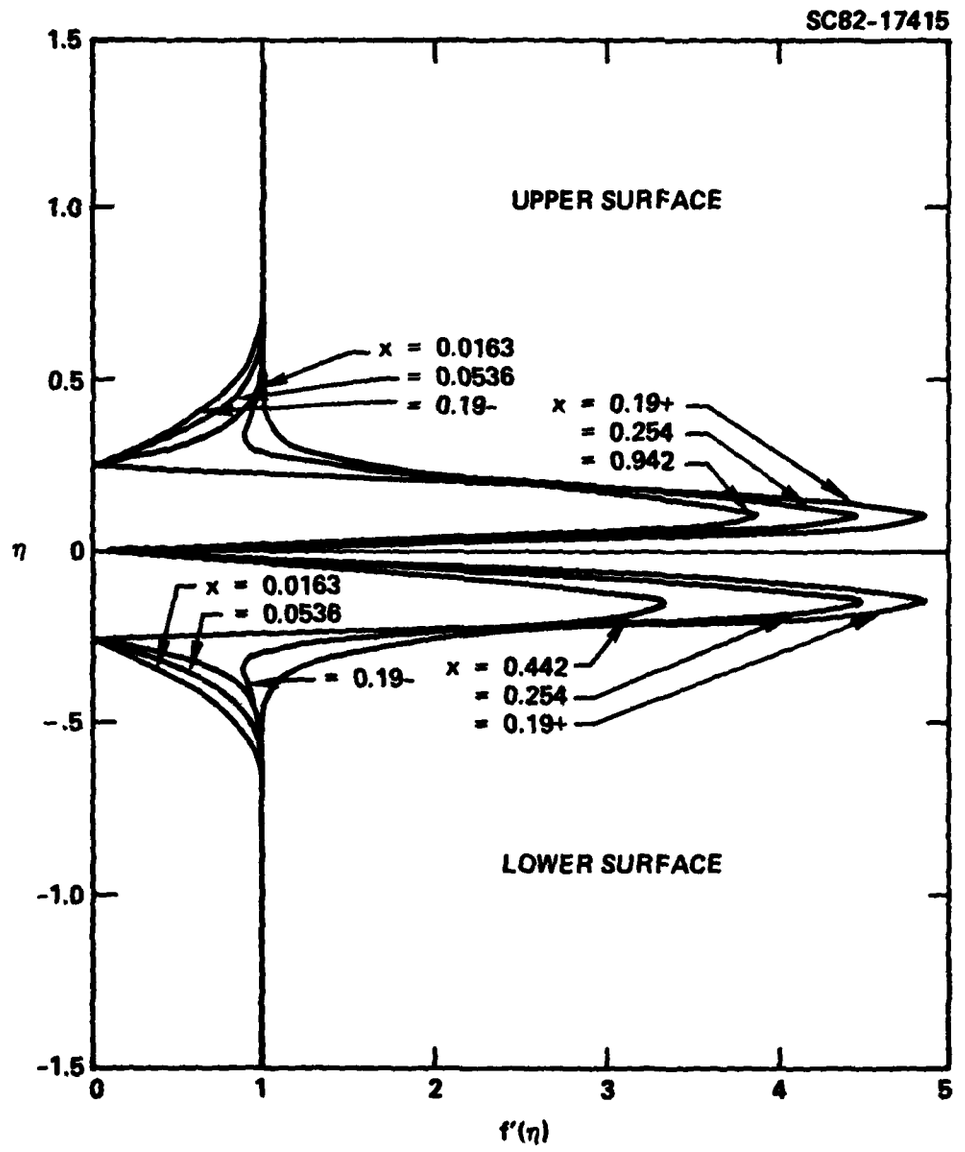

Fig. 5 Streamwise development of boundary layer and wall jet velocity profiles over airfoil. Profiles for upper surface shown in upper part of figure; lower surface values in lower part of figure.

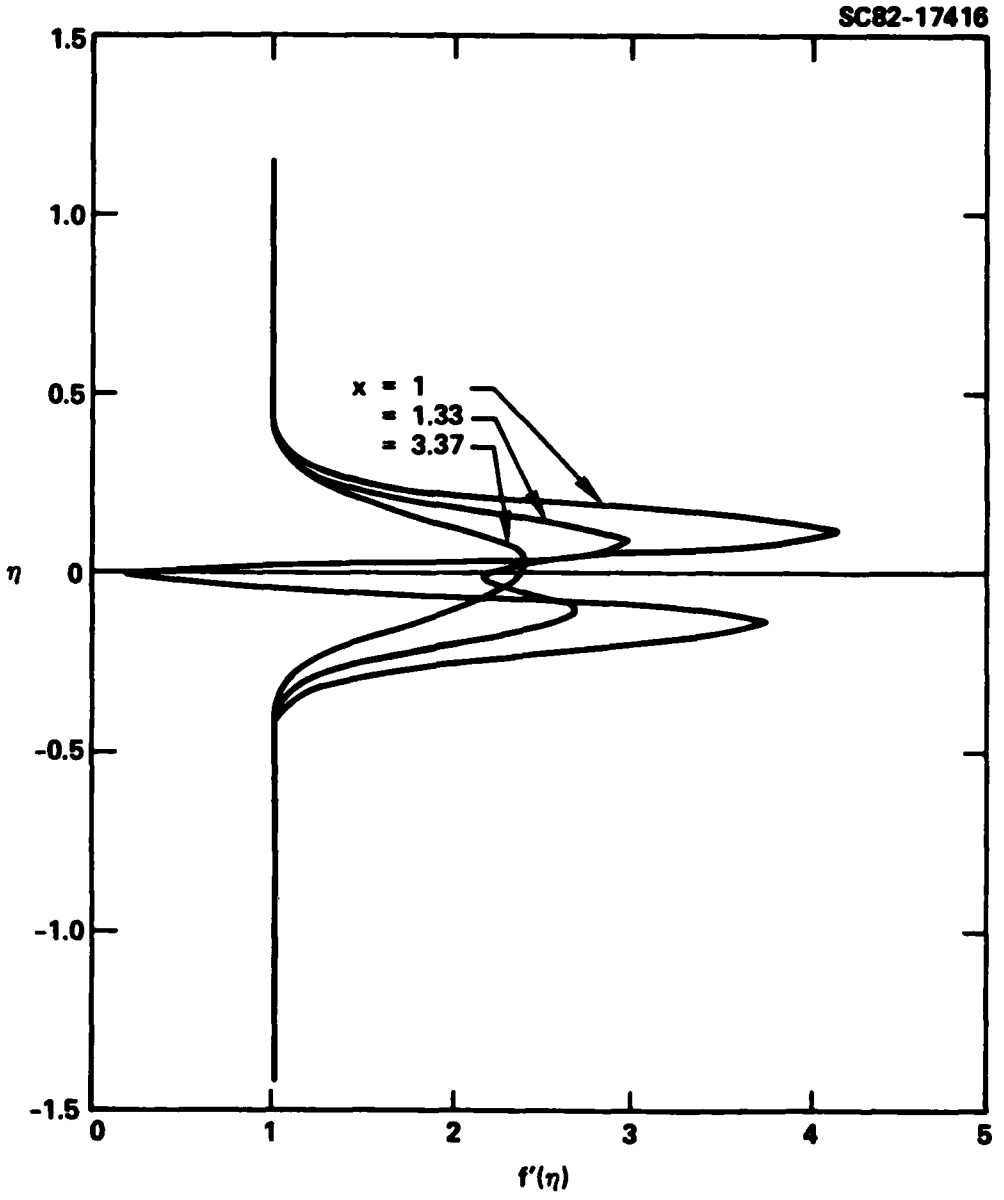

Fig. 6 Streamwise development of velocity profiles in wake for $M_\infty = 0.75$, $\alpha = 1^0$, $C_J = 0.055$.

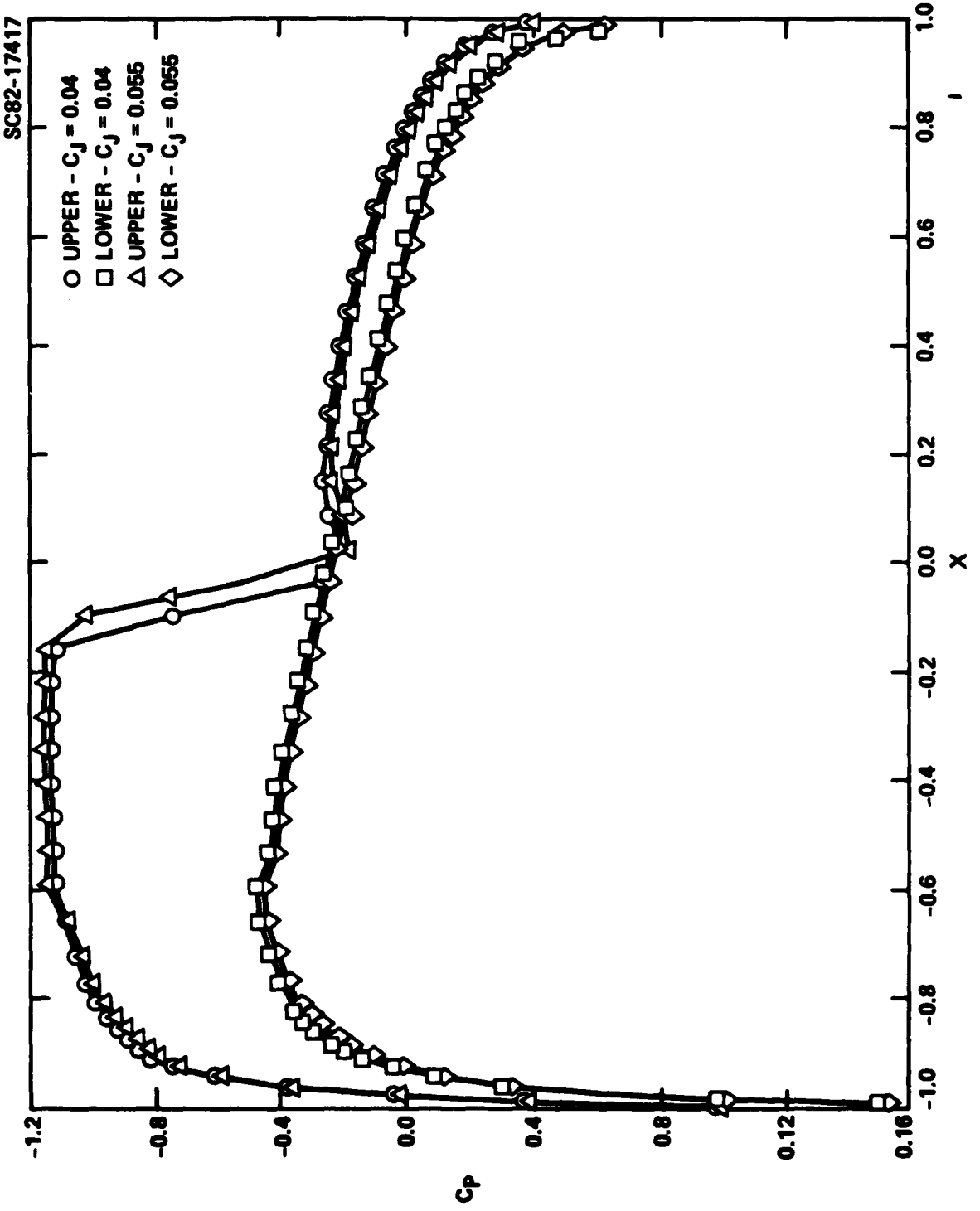

Fig. 7 Effect of blowing coefficient C_J on chordwise pressure distributions, $M_\infty = 0.75, \alpha = 1^0$.

$$H = \delta/\theta \tag{23b}$$

$$\tau = \mu \frac{\partial u}{\partial y}\Big|_{y=0} \tag{23c}$$

where the subscript e refers to the edge of the boundary layer, H is the shape factor, and M_e is the Mach number at the edge of the boundary layer. The numerical values obtained from the computational solutions satisfied (23) to within roughly the truncation error of the method. This served as a validation of our application of the box scheme to blown flows and also explained the negative values of $\theta'(x)$ on the blown portions of the airfoil. A key element in these considerations is that θ itself is negative in these regions, as has been previously observed. Thus, if $\theta < 0$ typified by the upstream portion of a wall jet, and an adverse pressure gradient is encountered, i.e., $\frac{du_e}{dx} < 0$, as in downstream of the terminating shock on the upper surface, then the pressure gradient term P will be negative. From (23a) it is obvious that if

$$|P| > C_f \quad ,$$

$\theta'(x)$ will also be negative.

Figure 4 exemplifies a situtation in which $\theta'(x)$ as well as $\delta^{*\prime}(x)$ is predominantly negative over most of the blown surface. Since the skin friction coefficient C_f can be influenced by the blowing coefficient C_J, cases can be conceived where the inequality (24) is reversed. This is also possible for turbulent flow. An an illustration, the algebraic eddy viscosity model of Patankar[23] and Ramaprian[24] given by Eqs. (15) was used to compute the turbulent analogue of the laminar flow considered herein. Figure 8 compares the chordwise pressures from laminar flow with the turbulent case, for following conditions: $M_\infty = 0.7$, $\alpha = 1°$, $C_J = 0.047$, $Re = 10^6$ and $x_{SL} = 0.19$. The inviscid solution is also displayed. In this mildly supercritical situation, it is evident from the figure that

SC82-17528

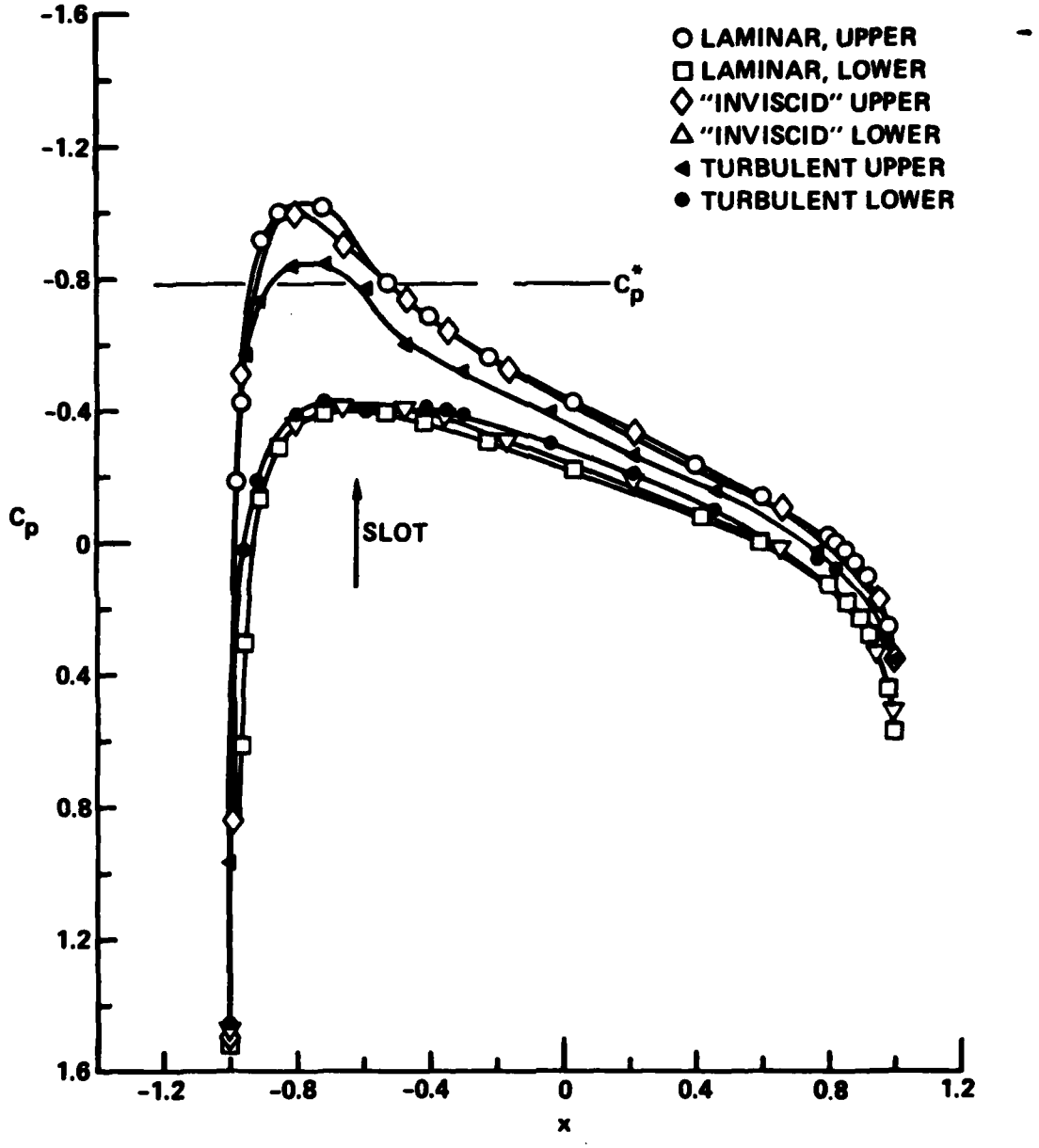

Fig. 8 Comparison of laminar and turbulent blown chordwise pressures with inviscid theory $M_\infty = 0.7, \alpha = 1^0, C_J = 0.047, Re = 10^6, x_{SL} = 0.19$, (NACA 0012 airfoil).

the laminar lifting pressures are greater than those predicted by the inviscid model. By contrast, the turbulent values are less, large differences occurring on the upper surface in the supersonic zone. The implication of this state of affairs with respect to overall forces is shown in Table 1.

TABLE 1. COMPARISON OF OVERALL FORCES ON BLOWN NACA 0012 AIRFOIL, $M_\infty = 0.7$, $\alpha = 1°$, $C_J = 0.047$, $Re = 10^6$, $x_{SL} = 0.19$

Mode	C_L	$C_{D_{WAVE}}$	C_{D_f}
Laminar	0.326	0.00716	0.0195
Turbulent	0.162	0.0129	0.0344
"Inviscid"	0.287	0.00611	—

To compute $C_{D_{WAVE}}$, the nose contribution near $x = 0$ is extremely important. Although the singular character discussed in connection with Eq. (20) could be used for this purpose, the numerical procedure given in Ref. 29 was found to be more convenient. The trends shown in Figure 8 and Table 1 can be more easily appreciated by reference to Figure 9 which displays the $\delta^*(x)$ distributions for the laminar and turbulent cases. On comparison of these variations, it is immediately obvious that the turbulent flow through the attendant larger values of C_f will at moderate distances downstream of the slot x_{SL} be governed by the inequality

$$|P| < C_f \quad , \tag{25}$$

the reverse of (24). According to (23a), $\theta'(x)$ becomes quickly positive, and since $H \approx 0.5$ or less, $\delta^{*\prime}$ exhibits a similar behavior*. By contrast

*Downstream, both terms of the right hand side of (23a) become positive.

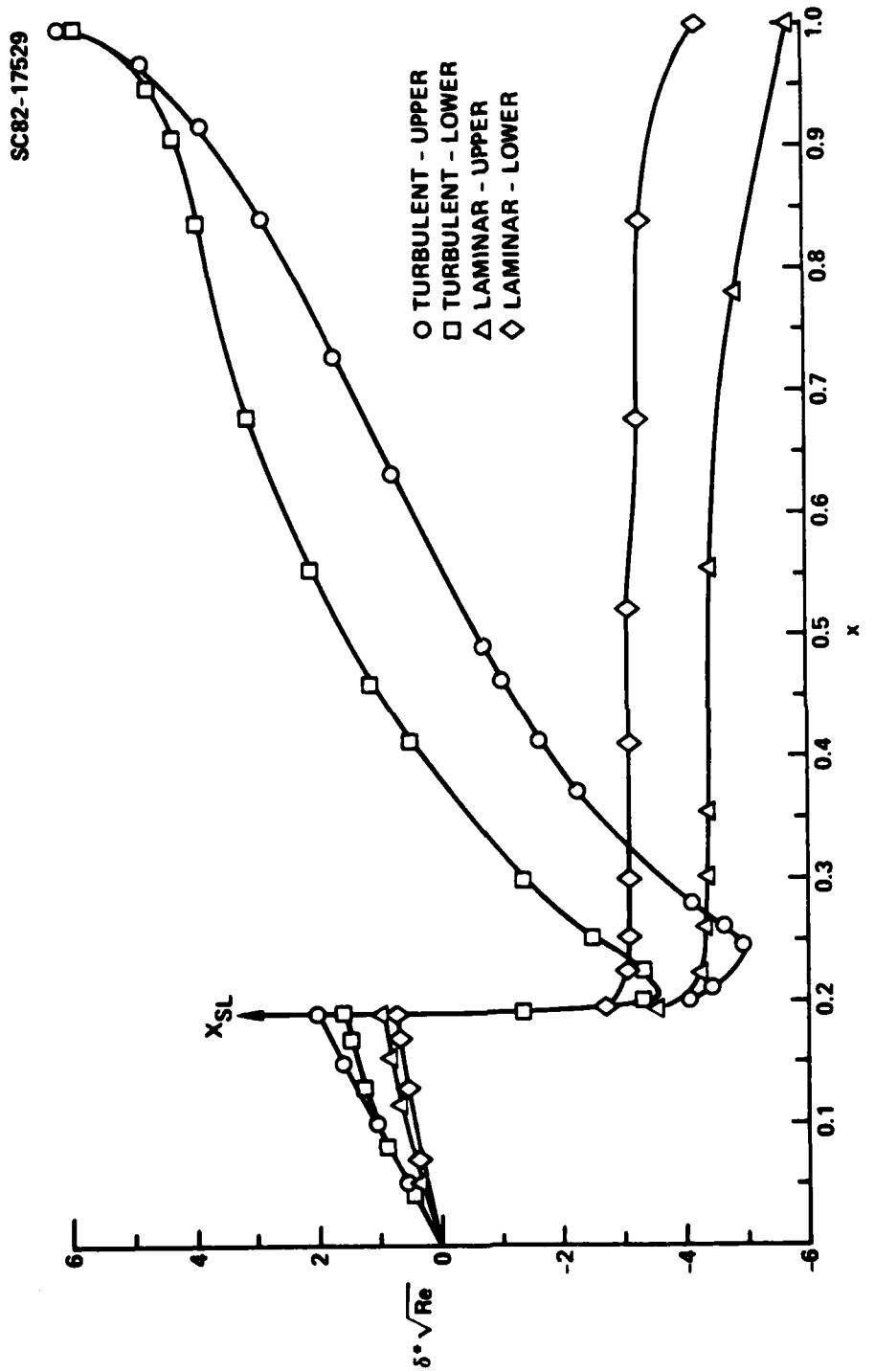

Fig. 9 Comparison of $\delta^*(x)$'s for turbulent and laminar flows, $M_\infty = 0.7$, $\alpha = 1^0$, $C_J = 0.047$, $Re = 10^6$, $x_{SL} = 0.19$, (NACA 0012 airfoil).

the laminar case as well as the one associated with Figure 4 satisfies (24), and accordingly, δ^* as well $\delta^{*\prime}$ are negative. Thus, the turbulent flow starts with an excess layer, but quickly transitions to a defect layer with its larger separation resisting shear stress at the wall, in contradistinction to the laminar case, which maintains the excess wall jet profile to the trailing edge with smaller surface shear stress. This increased C_f leads to the higher C_{D_f} shown in Table 1. Because $\delta^{*\prime}(x)$ becomes positive quickly downstream of the slot, the more separation resistant turbulent wall jet gives rise to the decambering effect and attendant lift loss described earlier. Furthermore, the profile thickening associated $\delta^{*\prime}(x) > 0$ results in greater wave drag than the laminar case as also shown in Table 1.

Returning to the laminar flow situation, and the effect of the viscous interaction processes on the overall force characteristics of blown airfoils, Figure 10 indicates the variations of wave drag coefficient $C_{D_{WAVE}}$ and friction drag C_{D_f} as a function of the blowing coefficient C_j. Various flight conditions are indicated, involving Mach numbers of 0.7 and 0.75 and incidences α of 1° and 2°, and a Reynolds number based on the airfoil chord of 10^6 as well as a slot location in units of the airfoil chord $x_{SL} = 0.19$. A striking and surprising linearity of C_{D_f} with C_j is apparent from these results. This behavior warrants further study. Comparable variations of C_j appear to provide considerably lower increases in wave drag $C_{D_{WAVE}}$ at a fixed M_∞,α combination. This trend which is believed to be typical for other airfoils is more clearly demonstrated in Figure 11 where the arrows there and subsequent plots indicate increasing C_j. From a practical engineering viewpoint, these numerical studies corroborate experimental evidence of a friction or "scrubbing" drag penalty associated with the separation delay or removal benefit of blowing. The computational model is general enough to provide cheap, systematic tradeoff studies to optimize a given airfoil. In this connection, the results of Figures 10 and 11 exemplify another important

SC82-17421

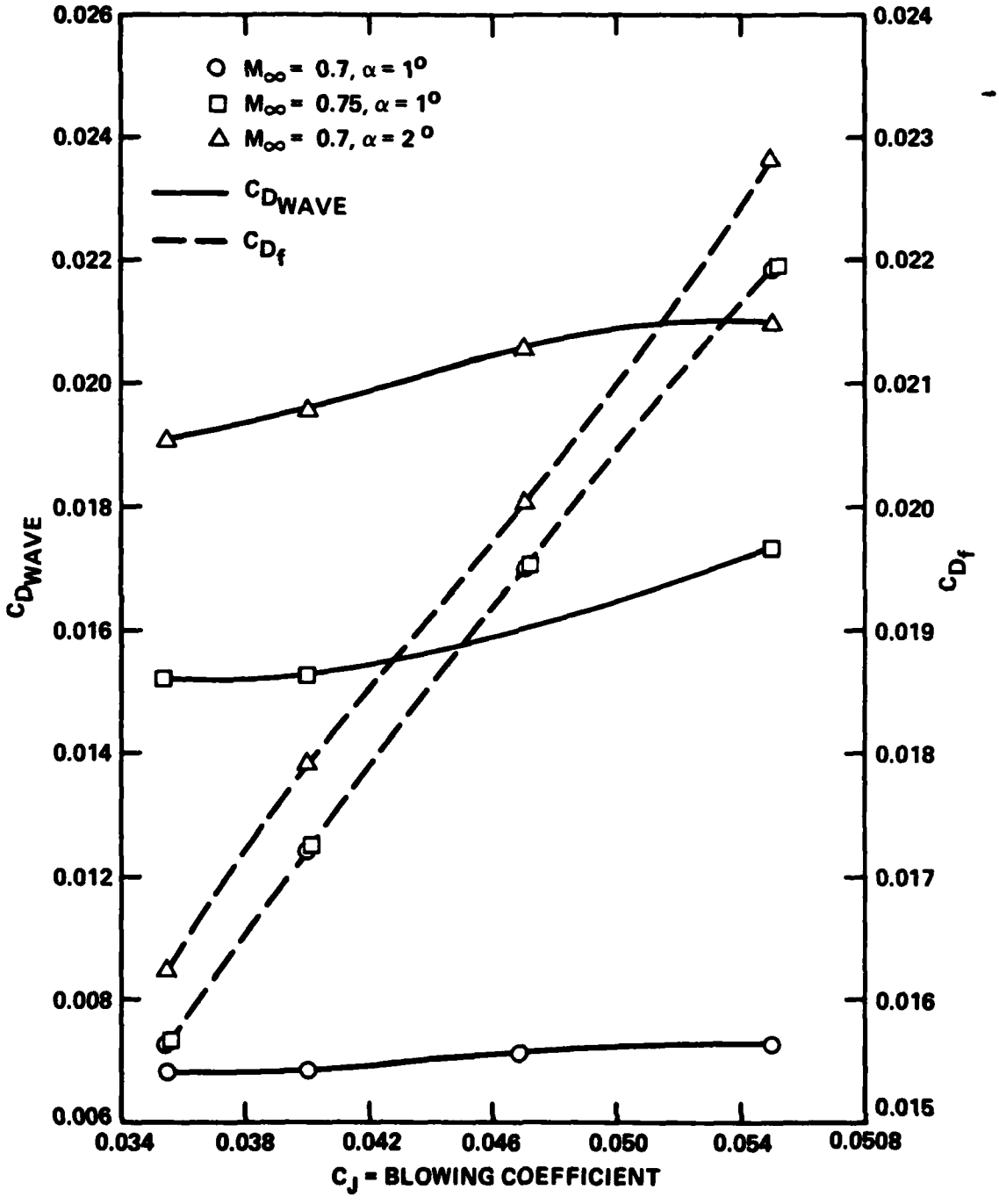

Fig. 10 Effect of blowing on drag coefficients.

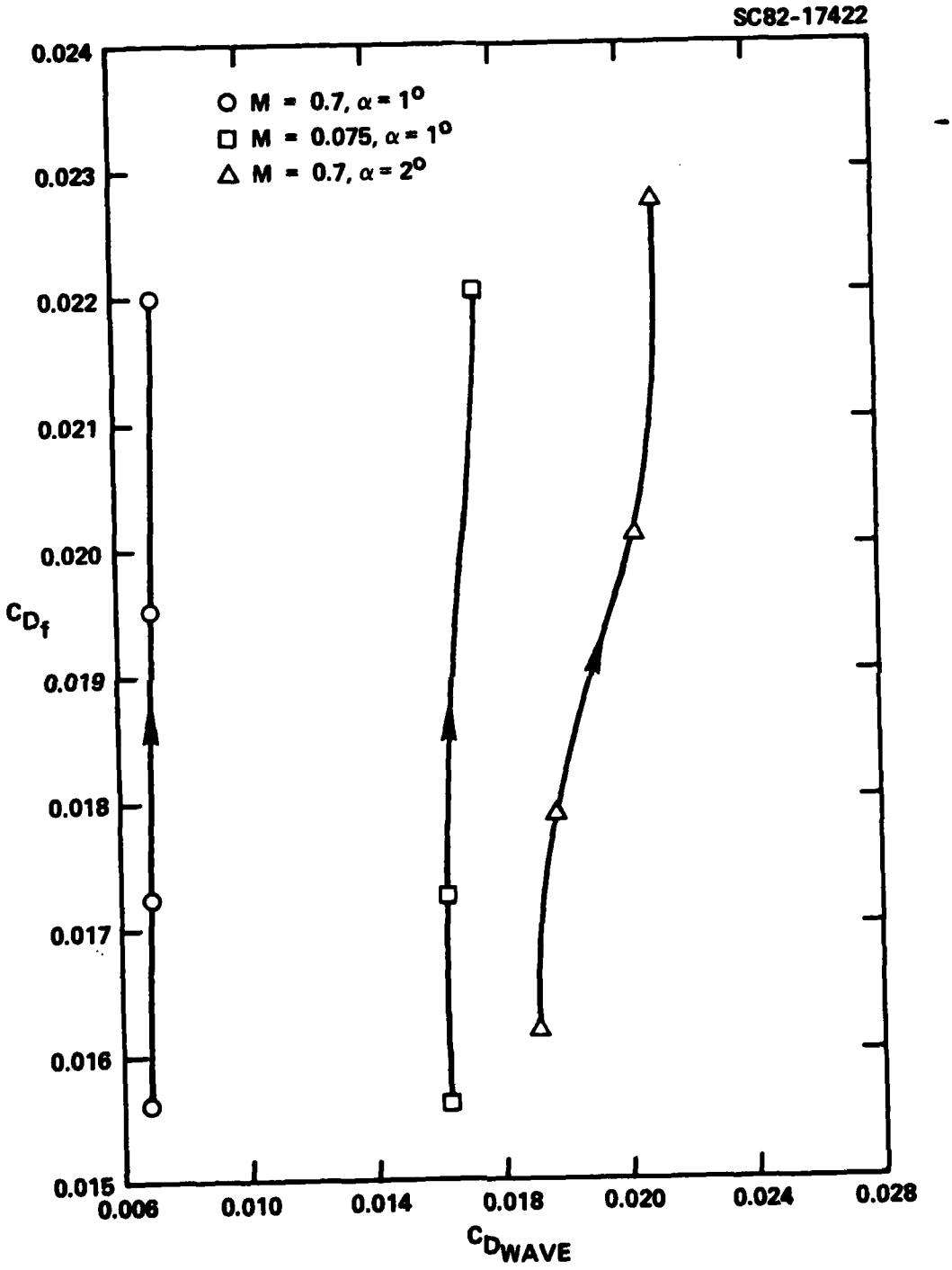

Fig. 11 Skin friction drag versus wave drag for varying blowing (arrows hereinafter denote blowing increasing).

trend, namely, the substantial increase in wave drag associated with increase in Mach number and incidence at a given blowing coefficient.

To obtain these results, a sequence of blowing coefficients was investigated which provided increasing lengths of separation-free flow over the airfoil until the trailing edge was reached. Defining the separation point $x = x_{sep}$ at which the shear stress vanishes or reverse flow is first encountered, the blowing coefficient was increased until the separation point reached the trailing edge, $x = 1$. For $x_{sep} < 1$, the weak viscous interaction model described in this report would not be applicable to describe the flow. In Ref. 6, the behavior of x_{sep} with C_j was indicated. Further studies of this trend were performed in this effort and some typical results are shown in Table 2 for a Reynolds number based on the airfoil chord of 10^6 for various slot locations.

TABLE 2. EFFECT OF BLOWING ON SEPARATION POINT, $M_\infty = 0.8$, $\alpha = 1°$

Case	C_j	x_{SL}	x_{sep}	x_S	x_1
6.2	0.047	0.14	0.859	0.796	0.793
8.3	0.03	0.14	0.793	0.766	0.732
8.1	0.0355	0.19	0.84264	0.766	0.782
9.1	0.04	0.19	0.84264	0.797	0.782
6.1	0.0398	0.10	0.81890	0.797	0.753
8.2	0.0257	0.10	0.81890	0.766	0.753

Indicated in the table for x_{sep} are locations of the x grid point closest to the separation location. This is evident in the computations when a divergence of the Newton iterations employed in the box scheme

occurs. This divergence is associated with incipient upstream flow or vanishing shear stress. Also tabulated are the locations x_s of the upstream (low pressure side) of the shock layer (which was spread ih the inviscid zeroth iterate over two to three points in the SOR grid), and x_1, the x location of the last box scheme point upstream of x_{sep}. From the results, it is evident that separation occurred close to the foot of the shock in these cases. The superficially puzzling invariance of x_{sep} to moderate changes in C_j for Cases 8.1, 9.1, 6.1 and 8.2 can be explained on the basis of the relative coarseness of the box scheme grid near the shock foot. It is evident from Table 2 that with the exception of Case 8.1 where the shock was upstream of the last box scheme grid point prior to separation, the shock was between this point and x_{sep}. With the relative coarseness of the box scheme grid in this location, it is conceivable that identical x_{sep} values could be obtained in the shock-induced adverse pressure gradient in this location.

Defining C_j^* as the blowing coefficient at which x_{sep} becomes unity as $C_j \rightarrow C_j^*$ from below, values of $C_j >> C_j^*$ ("overblowing") may be inefficient from an L/D, $C_{D_{WAVE}}$ and frictional or scrubbing drag viewpoint, despite supercirculation gains. In addition to Figure 10 and 11, the importance of frictional drag in relation to wave drag is shown in Figure 12. Although large increases in the friction drag were encountered with increases in C_j, the percentage of this mode to the total is not strongly influenced by the magnitude of the blowing coefficient. It is evident that the lower Mach number-incidence combinations lead to frictional drags of the order of 70 to 75% of the total, whereas for a modest increase in Mach number, it reduces to about half of the total. To our knowledge, these are the first quantifications of such trends from a computational model.

The variations of lift coefficient associated with overblowing are shown in Figure 13. Relatively small increases in lift are exhibited for appreciable increases in blowing. Such increases can lead to degradations

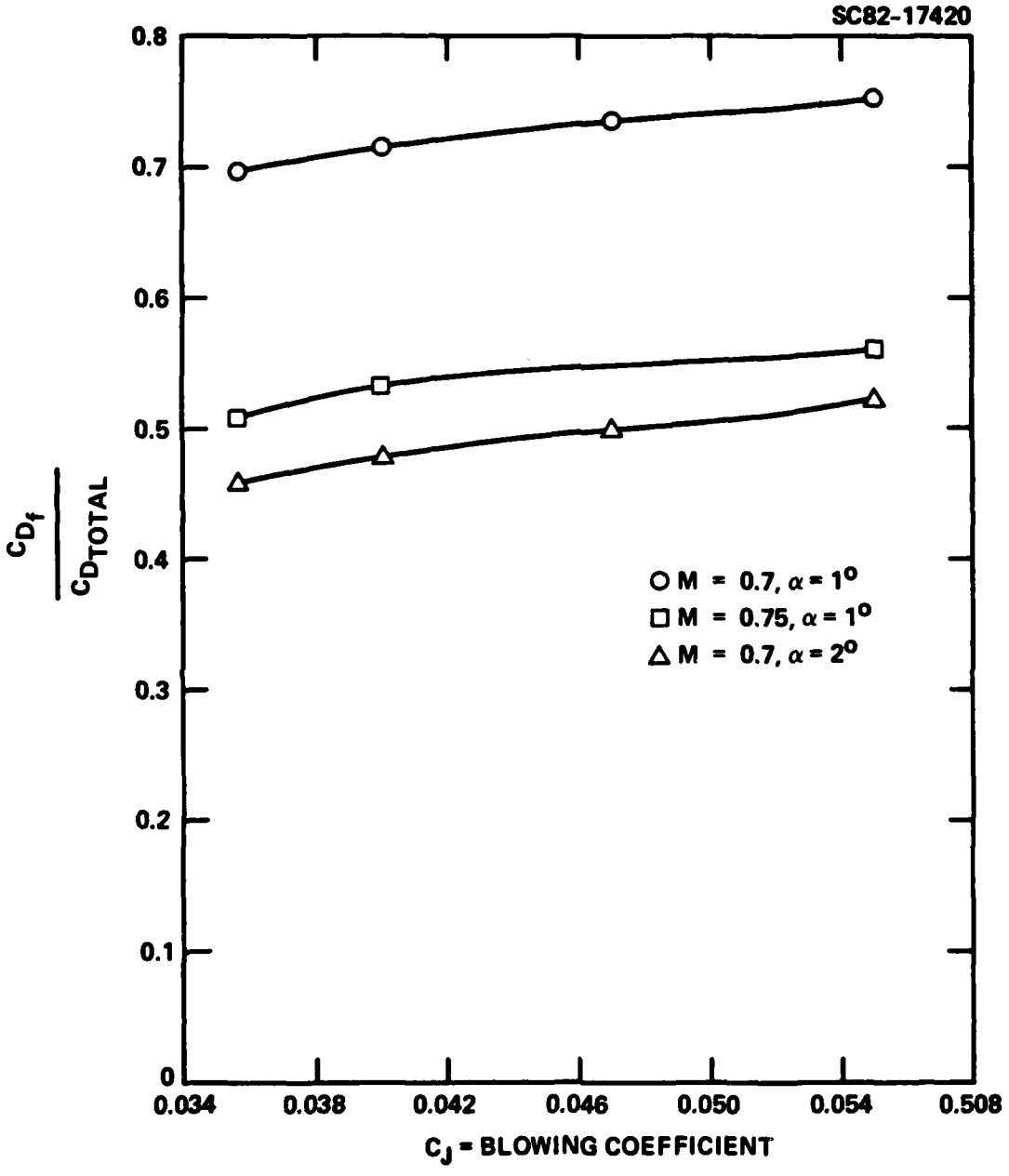

Fig. 12 Fraction of total drag associated with various blowing rates and flight conditions.

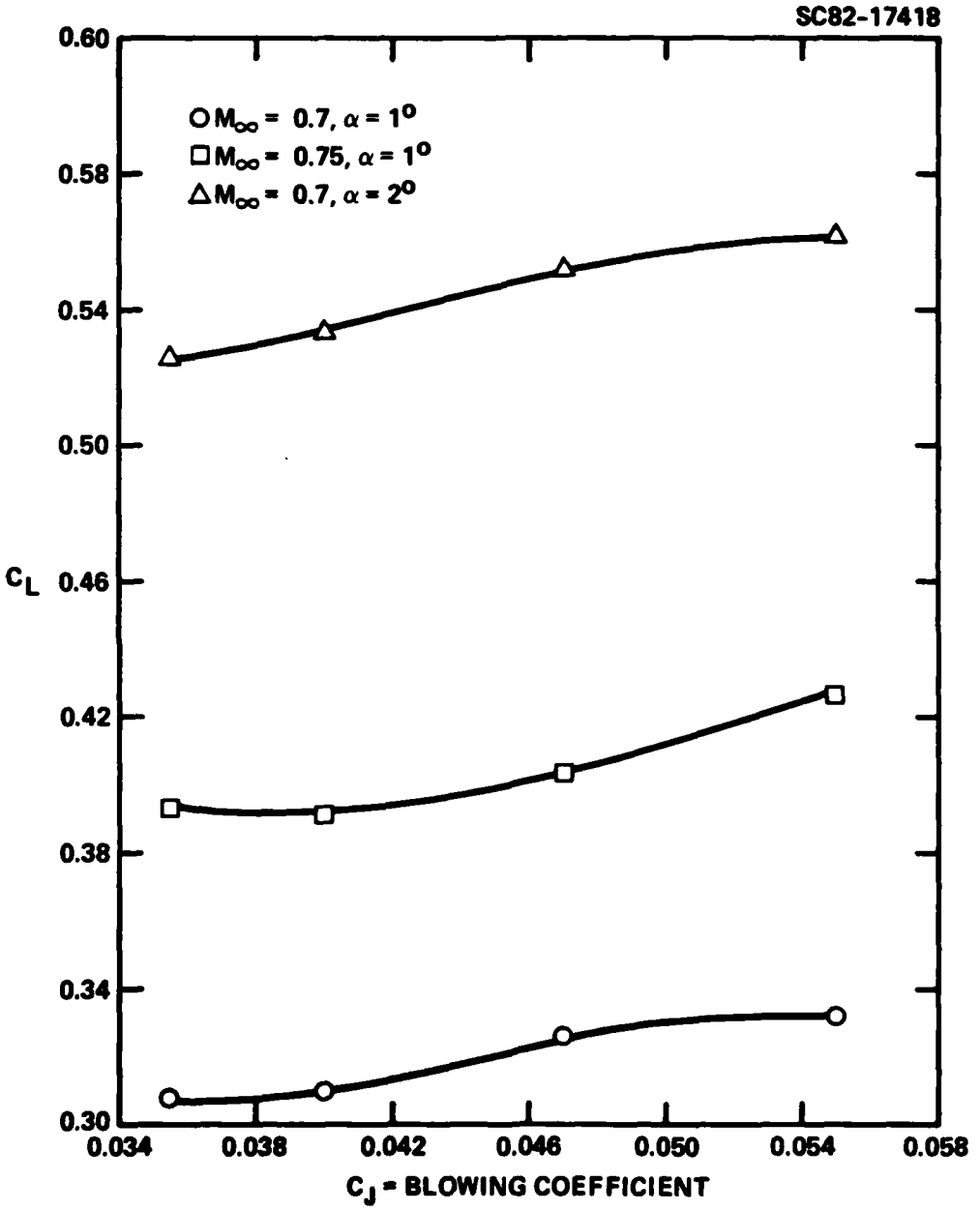

Fig. 13 Effect of blowing on lift.

in aerodynamic efficiency (L/D) as shown in Figures 14 and 15 for these blowing enhancements. Further elucidation of these trends is shown in Figure 16, where the L/D changes associated with lift gains are shown (setting aside the issue of trim drag). For the lower Mach number cases, within the C_j range assumed (which is somewhat greater than C_j^*), increases in lift give L/D loss. At the higher Mach number, an optimum C_L is shown for maximum L/D. It is interesting to note that this is obtained at the smallest C_j studied, i.e., 0.0355. Although the achievement of high lift is necessary for good turn performance, the significance of the L/D loss is important from the viewpoint of maintenance of constant altitude, speed, or specific power factor during maneuver scenarios.

In addition to the foregoing aspects, the viscous interaction model was used to study the effect of Reynolds number and slot location on aerodynamic characteristics as shown in Table 3*.

TABLE 3. EFFECT OF REYNOLDS NUMBER Re AND SLOT LOCATION ON AERODYNAMIC CHARACTERISTICS, $M_\infty = 0.75$, $\alpha = 1°$, $C_j = 0.0371$

Re	x_{SL}	C_{D_W}	C_{D_f}	C_L
10^6	0.10	0.0142	0.0177	0.531
10^7	0.10	0.0112	0.0144	0.360
10^7	0.25	0.0153	0.0152	0.383

With the increased Reynolds number, the friction drag and lift coefficient are reduced. This is in accord with the transpiration boundary condition modification effects previously described. The reduced lift is associated with a reduction of viscous camber and supercriticality at the higher Reynolds number. Associated diminished profile thinning

*For $x_{SL} = 0.10$, the "inviscid" results gave $C_{D_W} = 0.00863$ and $C_L = 0.322$, consistent with the Re trend shown in Table 3.

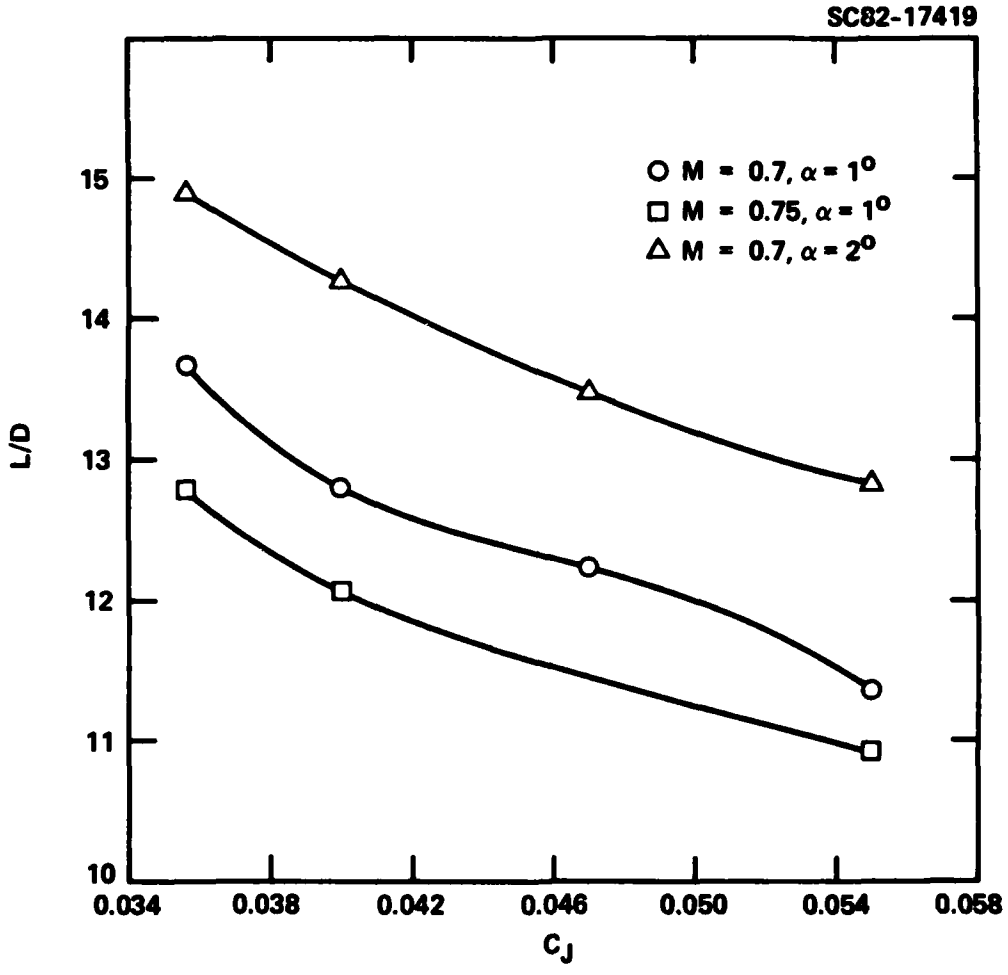

Fig. 14 Effect of blowing on $L/D = C_L/(C_{D_{wave}} + C_{D_f})$

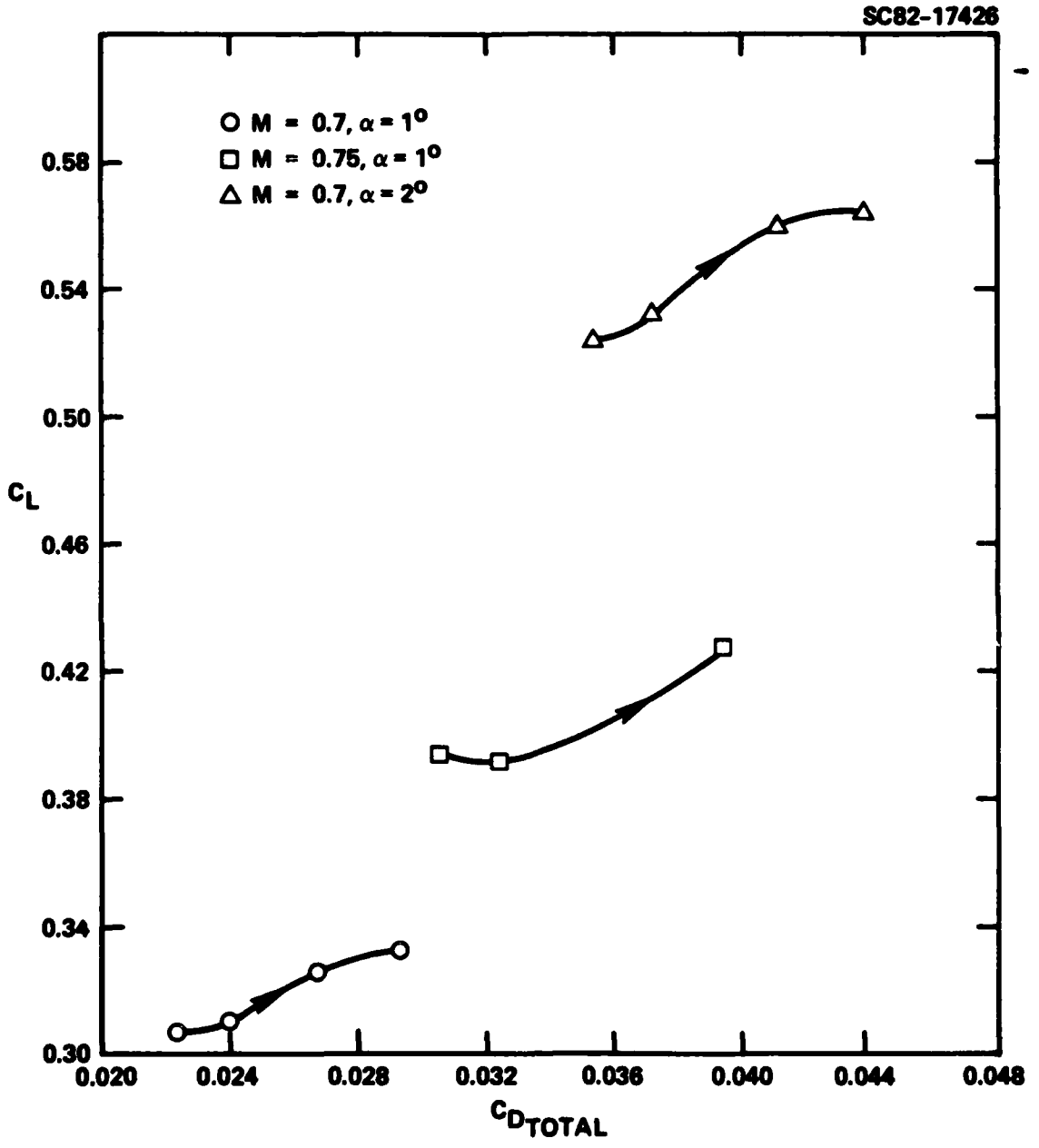

Fig. 15 Modifications of lift and drag with blowing.

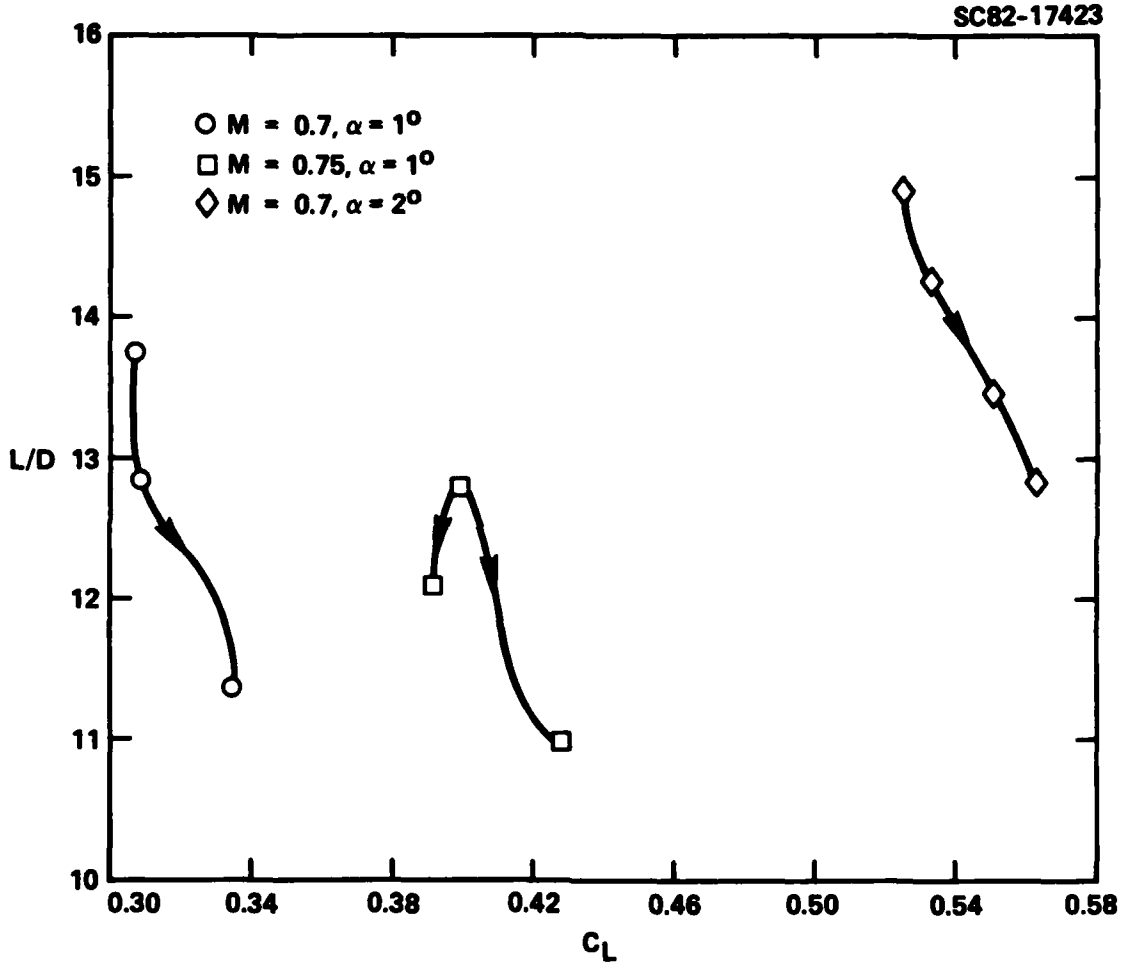

Fig. 16 Variation of aerodynamic efficiency with lift coefficient at various flight conditions.

reduces the wave drag. Table 3 also shows reduced friction drag associated with downstream movement of the slot for the same blowing coefficient. This is related to a smaller coverage of the enhanced frictional dissipation of the wall jet from the slot blowing. Since the net sink strength is less in proportion to the region covered, the effective thickness is greater, leading to increased wave drag and reduced lift with rearward slot movement.

From the model and the studies previously described, certain considerations emerge relevant to the design of optimum blown transonic airfoils. Important ones, we believe, are the following:

1. In addition to the possibility of high friction drag occurring with excessive overblowing, additional wave drag arises due to a cambering effect from the downward momentum imparted to the flow from the wall jets. To deal with this problem, inverse methods such as those developed in Ref. 19 generalized to the viscous interaction formulation given herein could lead to improved aerodynamic efficiencies associated with lift augmentation with blowing. The inverse procedure would be utilized to eliminate or suppress shock waves in the flow. In addition to the attendant wave drag reduction, there would also be an accompanying alleviation of the adverse pressure gradient creating separated flow. This modification would reduce the C_j required to achieve attached flow, in turn easing engine, structural, and heat transfer penalties as well as offsetting internal flow losses. Conversely, although increased blowing delays separation, there is a secondary counteractive effect involving the intensification of the shock (due to the induced camber), augmenting the adverse pressure gradient. This will degrade the effectiveness of the blowing to some extent.

2. The possibility of modifying transition and achieving laminar flow through tangential blowing is of some interest. One conceivable mechanism is through alteration of the velocity profiles. For unblown cases, Rayleigh's inviscid stability theory (see Ref. 30 for an account) indicates that a necessary condition for amplification of disturbances is the occurrence of a point of inflection in the velocity profile. In the case of monotonic velocity profiles, Rayleigh's inflection point theorem can be derived directly from the Sturm-Liouville problem related to a plane wave stability analysis. Based on this thinking, pressure gradient parameters and/or the shape factor H defined by the ratio of the displacement to momentum thickness can be correlated against the critical Reynolds number R_c for the inception of instability. In this context, it has been demonstrated theoretically and experimentally that favorable pressure gradients greatly enhance stability and unfavorable ones detract from it. Moreover, decreasing H toward 2 from about 3.6 has been shown to substantially increase R_c.

Application of item 2 to tangential blowing and wall jets has not been made to our knowledge, and leads to some difficulties. Superficially, it might be anticipated that blowing could be used to control the shape factor and through generalizations of the considerations associated with boundary layers, augment stability, with the ultimate application of laminarization of an airfoil. Indications of the alterations of the curvature of the velocity profiles and changes in the shape factor associated with the blown airfoil considered in this investigation are given in Figures 17 and 18. It is interesting to note that reflecting the excess velocity character of the wall jets on these airfoils, the shape factors shown in Figure 18 are nowhere in the range considered in the standard stability literature. In violation of the conditions of

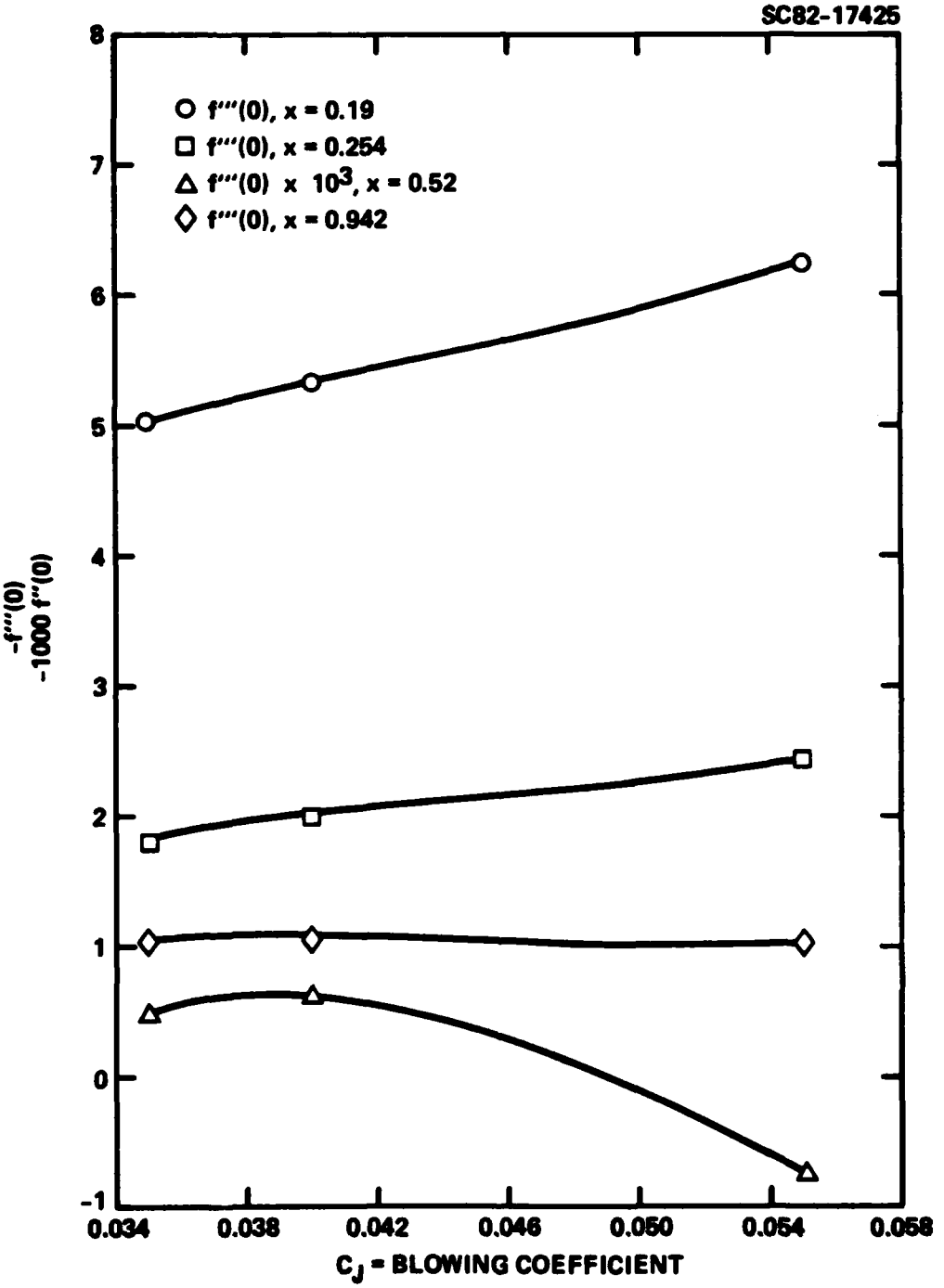

Fig. 17 Curvature of velocity profile at wall for varying blowing, $M_\infty = 0.75, \alpha = 1^0$, (upper surface).

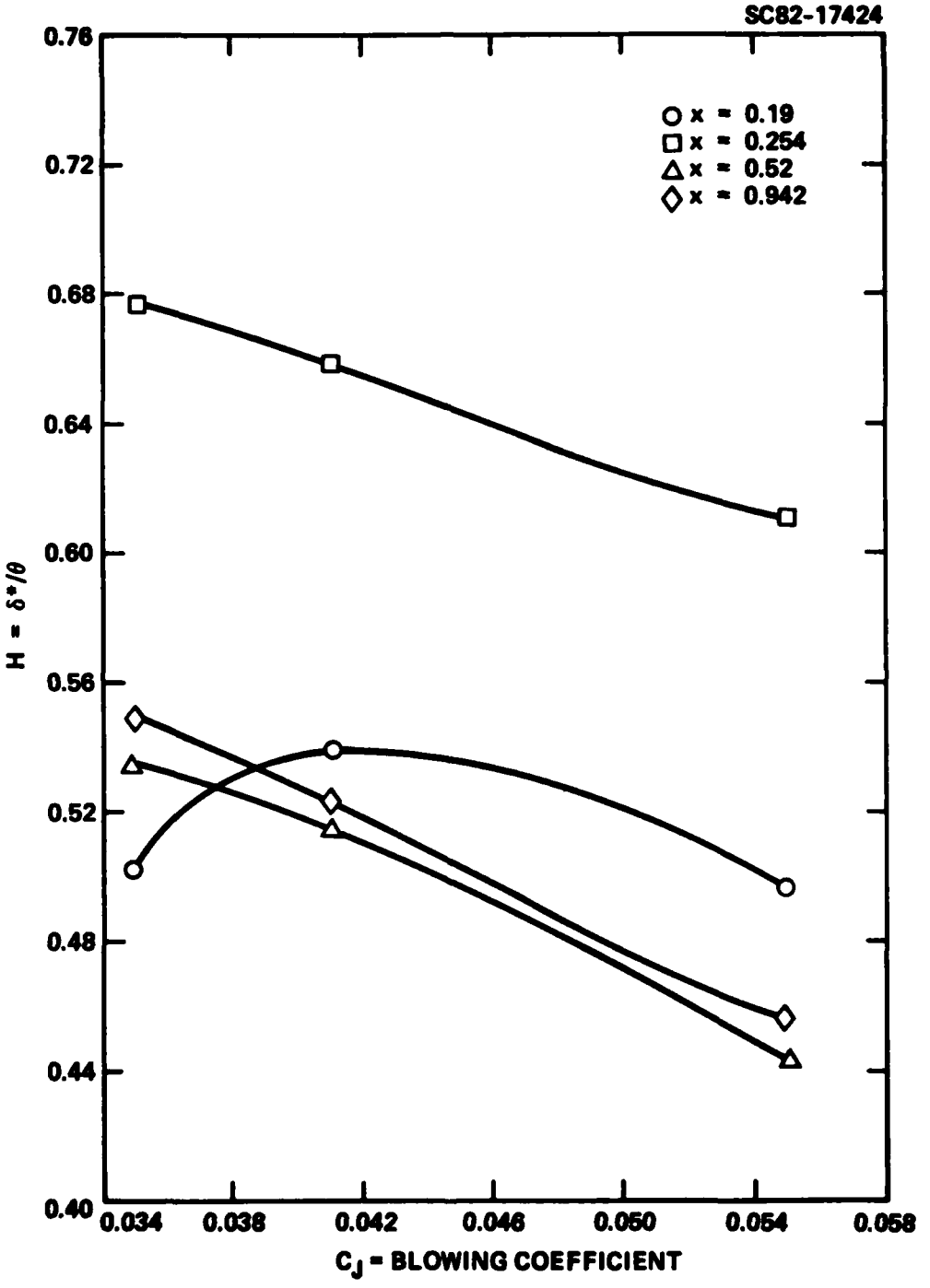

Fig. 18 Variation of shape factor, H downstream of slot (0.19ℓ) for NACA 0012 airfoil, $M_\infty = 0.75$, $\alpha = 1°$, (upper surface).

Rayleigh's theorem, the velocity profiles of wall jets are furthermore non-monotone in character. An additional set of practical complications deals with density variations in the hot engine gas used for the tangential blowing as well as upstream disturbances that could act as trips upon injection into the boundary layers. In spite of these difficulties, it is felt that this area is a fruitful one for future theoretical and experimental research. Regarding the former, a useful point of departure would be investigation of the stability properties of simple wall jets according to a generalization of the thinking leading to Rayleigh's theorem.

5.0 CONCLUSIONS

A viscous interaction model has been developed for the treatment of tangentially blown transonic airfoils. The coupling procedure employs a small disturbance approximation for the nearly inviscid outer flow and interacts this region with the boundary layers, wall jets and propulsive wake. The box scheme has been generalized to treat the latter, giving rapid convergence of the viscid-inviscid iterative sequence. Observations based on the parametric studies conducted indicate that for laminar flow:

1. The skin friction drag appears to increase nearly linearly with blowing coefficient C_J for a fixed Mach number-incidence combination giving a substantial "scrubbing" drag penalty for overblowing beyond the $C_J = C_J^*$ necessary to achieve attached flow.

2. Wave drag increases are much smaller than those for skin friction over the same range of increase of C_J.

3. The viscous interactions move the terminating shock of the supersonic region rearward with respect to its inviscid position. There is an attendant increase in lift and supercriticality with the viscous interactions.

4. The computational model can quantify the rearward movement of the separation point with increases in C_J and thereby be used to size the thrust bleed requirements for maintenance of attached flow. Other trade-offs are also easily accessible using the simulation.

5. Although large increases in friction drag were encountered with moderate increases in C_J at a given Mach number and

incidence, the percentage of the friction drag to the total drag is not strongly influenced by C_J over the range considered.

6. For a fixed C_J, the percentage of friction drag to the total drag tends to decrease at higher Mach number-incidence combinations, presumably reflecting the attendant disproportionate increases in wave drag.

7. The supercirculation gains associated with overblowing ($C_J > C_J^*$) do not provide large increases in the aerodynamic efficiency (L/D) due to the scrubbing drag referred to in Item 1.

8. Increased Reynolds number leads to decreases in the lift augmentation associated with viscous interaction effects as well as reduced friction and wave drag.

9. Downstream slot movement increases the wave drag, as well as reducing the skin friction drag and lift. This is particularly important from a design viewpoint with respect to minimization of the scrubbing drag.

10. Studies based on an algebraic turbulence model employed in the viscous interaction algorithm suggest that the lift decreases from values predicted by the inviscid model in contrast to the increases in the laminar case. There is also an attendant increase in frictional and wave drags. This behavior can be explained from the presence of greater friction, which reverses the laminar negative streamwise gradient of displacement thickness downstream of the injection slot, decambering the airfoil as in the

case of a conventional boundary layer and in contrast to the cambering effect of laminar blowing. The reversal, which is observed from the computational solutions can be explained in terms of the Karman integral momentum equation. Thus, the enhanced resistance to separation within the turbulent framework is accompanied by a degradation of aerodynamic characteristics as compared to laminar flow.

6.0 RECOMMENDATIONS

On the basis of the foregoing discussion, it is evident that a number of important areas should be addressed to understand and exploit tangential blowing procedures for the improvement of the aerodynamic performance of wings. From a modeling viewpoint, the scheme discussed applies certain approximations at the slot, trailing edge, and far field.

In the vicinity of the slot, the boundary layer assumptions break down and wave interactions can play a key role in providing the appropriate initial conditions for the ensuing downstream boundary layer development. In this vicinity, waves may reflect or transmit through the mixing layer modifying the external flow and the wall jet. The asymptotic procedures formulated in Ref. 6 should be further generalized and computationally applied to treat these interactions. This analysis could be useful in determining the slot location optimizing separation prevention and aerodynamic characteristics.

Near the trailing edge, local solutions which are essentially a generalization of existing multiple-deck methods for blowing should be developed. The implications of this refinement with respect to the Kutta condition and lift augmentation should be assessed. In spite of recent work on the near wake, there appears to have been no treatments of cases in which the shock is near the trailing edge or the latter is close to critical conditions even for the unblown case. This situation occurs frequently in practice, and a detailed analysis of it generalized to blowing would have great impact.

The analysis in this report utilizes a far field based on circulation theorems for viscous two-dimensional flow and heuristic considerations. A systematic asymptotic treatment involving matching, highlighting the role of viscous effects on the vorticity in the wake as well as the development of the supercirculation field with blowing would be an extremely useful analysis. It would provide further insight

into the mechanisms associated with thrust recovery as well as illuminate the structure of blown flow fields.

From a practical viewpoint, the simultaneous use of an inverse method with the viscous-interaction model could substantially offset the wave drag penalty associated with blowing strong enough to prevent separation. Further effort along these lines is therefore recommended.

In addition to the foregoing, application of blowing an three-dimensional configurations leads to other important issues. Some of these are related to further compromises required to deal with vortex drag in addition to wave and friction forms, as well as the possibilities of exploitation of favorable interference effects interacting with those from blowing to optimize aerodynamic performance. Examples of the latter are blown canard-wing arrangements, in which the blowing can offset adverse pressure gradients induced by the canard induction on the wing transonically and yet preserve low speed stall alleviation through vortex interactions.

7.0 REFERENCES

1. Spence, D.A., "The Lift Coefficient of a Thin Jet Flapped Wing," Proceedings of the Royal Society, Ser. A, Vol. 238, December 1956, pp. 46-68.

2. Bevilaqua, P., "Progress Toward a Theory of Thrust Recovery," AFOSR Final Report (1981).

3. Malmuth, N.D. and Murphy, W.D., "A Relaxation Solution for Transonic Flow over Jet Flapped Airfoils," AIAA Journal, Vol. 14, No. 9, September 1976, pp. 1250-1257.

4. Murphy, W.D. and Malmuth, N.D., "A Relaxation Solution for Transonic Flow over Three-Dimensional Jet-Flapped Wings," AIAA Journal, Vol. 15, No. 1, January 1977, pp. 46-53.

5. Malmuth, N.D., Murphy, W.D., Shankar, V., Cole, J.D. and Cumberbatch, E. "Upper Surface Blown Airfoils in Incompressible and Transonic Flows," AIAA Journal, Vol. 119, No. 12, December 1981, pp. 1501-1512. Also AIAA Paper 80-0270, AIAA 18th Aerospace Sciences Meeting, Pasadena, California, January 14-16, 1980.

6. Malmuth, N.D., Murphy, W.D., and Cole, J.D., "A Study of Wall Jets and Tangentially Blown Wings," Report No. SC5055.21FR, Rockwell International Science Center, Final Report, ONR Contract N00014-76-6-0350, July 1981.

7. Malmuth, N.D., Murphy, W.D., Shankar, V., Cole, J.D., and Cumberbatch, E., "Flow Structures Associated with Upper Surface Blown Airfoils," Invited paper presented at the Symposium on Numerical and Physical Aspects of Aerodynamic Flows, California State University, Long Beach, California, January 19-21, 1981, in proceedings and to be published by Springer Verlag.

8. Lock, R.C., "Calculation of Viscous Effects on Airfoils in Compressible Flow," Royal Aircraft Establishment Tech. Memo AERO 1646, September 1975.

9. Firmin, M.C.P. and Jones, A.F., "The Calculation of Pressure Distribution, Lift and Drag on Single Aerofoils at Supercritical Speeds," Royal Aircraft Establishment Tech. Memo, 1974.

10. Hall, M.G. and Firmin, M.C.P., "Recent Developments in Methods for Calculating Transonic Flows over Wings," ICAS Paper 74-18, 1974.

11. Lock, R.C., "A Review of Methods for Predicting Viscous Effects on Aerofoils and Wings at Transonic Speeds," Computation of Viscous-Inviscid Interactions, AGARD Conference Proceedings No. 291, Colorado Springs, Colorado, September 29 - October 1, 1980.

12. Le Balleur, J.C., "Calcul des Ecoulements a Forte Interaction Visqueuse au moyen de Methods de Couplage," loc. cit.

13. Keller, H.B. and Cebeci, T., "Accurate Numerical Methods for Boundary-Layer Flows. II: Two-Dimensional Turbulent Flows," AIAA Journal, Vol. 10, No. 9, September 1972, pp. 1193-1199.

14. Keller, H.B., "A New Difference Scheme for Parabolic Problems," Numerical Solution of Partial Differential Equations, Vol. II edited by J. Bramble, Academic Press, New York, 1970.

15. Cebeci, T., Kaups, K., and Ramsey, J.A., "A General Method for Calculating Three-Dimensional Compressible Laminar and Turbulent Boundary Layers on Arbitrary Wings," NASA Tech. Report CR-2777, January 1977.

16. Murphy, W.D., Shankar, V., and Malmuth, N.D., "A Computational Model for Three-Dimensional Incompressible Wall Jets with Large Cross Flow," Workshop on Thrust Augmenting Ejectors, Ames Research Center, Moffett Field, California, June 28-29, 1978, NASA Conference Publication 2093, September 1979.

17. Jameson, A., "Iterative Solution of Transonic Flows over Airfoils and Wings, Including Flows at Mach 1," Comm. Pure Applied Math., Vol. 27, 1974, pp. 283-309.

18. Murman, E.M. and Cole, J.D., "Calculation of Plane Steady Transonic Flows," AIAA Journal, Vol. 9, No. 1, January 1971, pp. 114-121.

19. Shankar, V., Malmuth, N.D. and Cole, J.D., "Computational Transonic Inverse Procedure for Wing Design with Automatic Trailing Edge Closure," to appear in AIAA J. (August 1982).

20. Thwaites, B., Incompressible Aerodynamics, Oxford, 1960, pp. 192, 194.

21. Lagerstrom, P.A., "Laminar Flow Theory," Theory of Laminar Flows, Volume IV, High Speed Aerodynamics and Jet Propulsion, Princeton University Press, Princeton, N.J., 1964, p. 55.

22. Stewartson, K., "On the Flow Near the Trailing Edge of a Flat Plate II," Mathematika, 16, (1969).

23. Patankar, S.V. and Spalding, D.B., "A Finite Difference Procedure for Solving the Equations of Two-Dimensional Boundary Layer," Int. J. Ht and Mass Transf., 10, 1967, pp. 1389-1411.

24. Ramaprian, B.R., "Turbulent Wall Jets in Conical Diffusers," AIAA J., 11, 10, December 1973, pp. 1684-1690.

25. Guderley, G., "The Flow Over a Flat Plate with Small Angle of Attack at Mach Number 1," J. Aero Sci, 21 (1954), pp.261-274.

26. Cebeci, T., Keller, H.B., and Williams, P.G., "Separating Boundary-Layer Flow Calculations," J. Comp. Phys., 31, 1979, pp. 363-378.

27. Cebeci, T., private communication.

28. Cebeci, T., Theile, F., Williams, P., and Stewartson, K., "On the Calculation of Symmetric Wakes I. Two-Dimensional Flows," Numerical Heat Transfer 2, (1979), pp. 35-60.

29. Murman, E.M., "Analysis of Embedded Shock Waves Calculated by Relaxation Methods," Proceedings of AIAA Computational Fluid Dynamics Conference, Palm Springs, California, July 1973,pp. 27-40.

30. Rosenhead, L., Laminar Boundary Layers, Oxford, (1963).

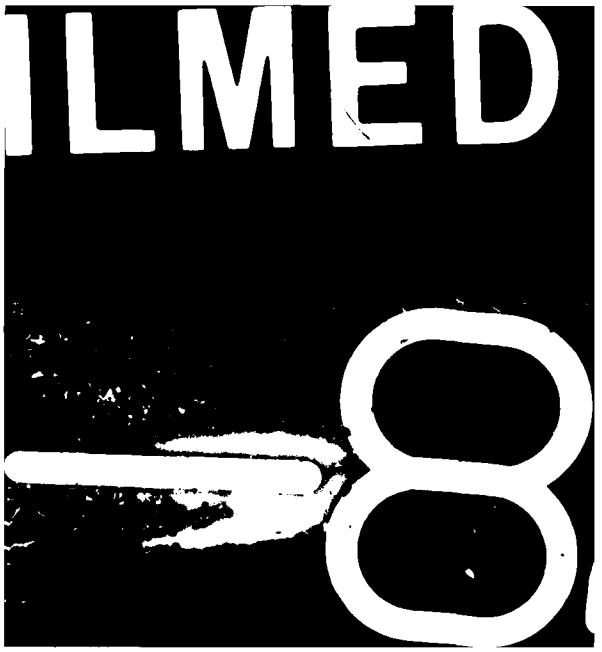
ILMED
8